EUROPEAN RESPIRATORY *journal*

FLAGSHIP SCIENTIFIC JOURNAL OF ERS

Early View

Original article

Eosinophils, Basophils, and Type 2 Immune Microenvironments in COPD-Affected Lung Tissue

Prajakta Jogdand, Premkumar Siddhuraj, Michiko Mori, Caroline Sanden, Jimmie Jönsson, Andrew F. Walls, Jennifer Kearley, Alison A. Humbles, Roland Kolbeck, Leif Bjermer, Paul Newbold, Jonas S. Erjefält

Please cite this article as: Jogdand P, Siddhuraj P, Mori M, *et al*. Eosinophils, Basophils, and Type 2 Immune Microenvironments in COPD-Affected Lung Tissue. *Eur Respir J* 2020; in press (https://doi.org/10.1183/13993003.00110-2019).

Eosinophils, Basophils, and Type 2 Immune Microenvironments in COPD-Affected Lung Tissue

Prajakta Jogdand[1], Premkumar Siddhuraj[1], Michiko Mori[1], Caroline Sanden[1,2], Jimmie Jönsson[2], Andrew F. Walls[3], Jennifer Kearley[4], Alison A. Humbles[4], Roland Kolbeck[4], Leif Bjermer[5], Paul Newbold[6], Jonas S. Erjefält[1,5]

[1]Department of Experimental Medical Science, Lund University, Sweden; [2]Medetect AB, Lund, Sweden; [3]Clinical and Experimental Sciences, University of Southampton, Southampton General Hospital, Southampton, UK; [4]Department of Respiratory, Inflammation and Autoimmunity, AstraZeneca, Gaithersburg, MD, USA; [5]Department of Respiratory Medicine and Allergology, Lund University, Lund, Sweden; [6]Department of Translational Sciences, AstraZeneca, Gaithersburg, MD, USA

Corresponding author:

Professor Jonas S. Erjefält

Unit of Airway Inflammation, BMC D12

Lund University

SE-221 84, Lund, Sweden

Telephone: +46-46-222-0960

E-mail: jonas.erjefalt@med.lu.se

Take-home message (248 characters with spaces; max 256): We identified highly localised Th_2 and eosinophil-rich pockets in COPD-affected lungs, which increased in number with increasing disease severity and included basophils. This exemplifies a novel type of heterogeneity in the immunopathology of COPD.

Keywords: COPD, eosinophils, basophils, viruses, chemokine CCL11/24

Word count: 3,359 (Maximum 3,000)

Figures: 7 (maximum 8 figures/tables)

ABSTRACT (199/200 words)

Although elevated blood or sputum eosinophils are present in many patients with chronic obstructive pulmonary disease (COPD), uncertainties remain regarding the anatomical distribution pattern of lung-infiltrating eosinophils. Basophils have remained virtually unexplored in COPD. This study mapped tissue-infiltrating eosinophils, basophils, and eosinophil-promoting immune mechanisms in COPD-affected lungs.

Surgical lung tissue and biopsies from major anatomical compartments were obtained from COPD patients with severity grades GOLD I–IV; never-smokers/smokers served as controls. Automated immunohistochemistry and *in-situ* hybridization identified immune cells, the type 2 immunity marker GATA3, and eotaxins (CCL11, CCL24).

Eosinophils and basophils were present in all anatomical compartments of COPD-affected lungs and increased significantly in very severe COPD. The eosinophilia was strikingly patchy, and focal eosinophil-rich microenvironments were spatially linked with $GATA3^+$ cells, including Th_2 lymphocytes and type 2 innate lymphoid cells. A similarly localised and IL-33/ST2-dependent eosinophilia was demonstrated in influenza-infected mice. Both mice and patients displayed spatially confined eotaxin signatures with $CCL11^+$ fibroblasts and $CCL24^+$ macrophages.

In addition to identifying tissue basophilia as a novel feature of advanced COPD, the identification of spatially confined eosinophil-rich type 2 microenvironments represents a novel type of heterogeneity in the immunopathology of COPD that will likely have implications for personalised treatment.

INTRODUCTION

Chronic obstructive pulmonary disease (COPD) impacts on global morbidity and mortality [1]. Underlying the disease is chronic inflammation leading to bronchitis, bronchiolitis, and emphysema resulting from long-term exposure to inhaled irritants (e.g., tobacco smoke) [2, 3]. COPD pathology has traditionally been attributed to innate immune mechanisms [3], but adaptive immune mechanisms are also activated [4, 5]. The immunopathology is further complicated by a marked heterogeneity in granulocyte profiles, with an increased attention to eosinophil signatures in COPD [6, 7]. Several studies have demonstrated high blood and/or sputum eosinophil counts in a significant percentage of patients with COPD [6–8]. Cluster analysis of sputum granulocyte profiles has also proposed eosinophil-rich sputum eosinophilia as a sign of a distinct eosinophil COPD phenotype [9].

Type 2 cytokines, particularly interleukin-5 (IL-5), are crucial for eosinophil development, maturation, and tissue longevity [10, 11]. This IL-5 dependence has been the rationale for targeting eosinophil-high COPD with neutralizing anti–IL-5 (mepolizumab) and anti–IL-5 receptor alpha (IL-5Rα; benralizumab) antibodies [12, 13]. Basophils also express IL-5Rα and are affected by IL-5/IL-5Rα blockade [14]. However, limited data exist on the tissue infiltration pattern and density of basophils in COPD-affected lungs.

Lung tissue-infiltrating eosinophils in COPD remains largely unexplored. Previous studies have confirmed eosinophil presence in central and distal compartments [15, 16]. However, important questions remain about the anatomical localization and infiltration patterns and the theoretical underpinning for eosinophilia in COPD and its immunologic triggers. Although type 2 cytokines

are classically from antigen-activated $CD4^+$ Th_2 lymphocytes, eosinophilia may develop through activated type 2 (ILC2) innate lymphoid cells [17–19], which upon activation (e.g., by IL-33) can rapidly mount a transient type 2 response [17, 18]. However, it remains to be demonstrated if ILC2 cells are present in tissues with eosinophilia in COPD-affected lungs. Eosinophil chemoattractant molecules in COPD also require investigation.

The aim of this study was to perform holistic spatial mapping of tissue-infiltrating eosinophils in COPD-affected lungs at different disease stages, and to identify key immunologic mechanisms thought to promote tissue eosinophilia. The investigation involved key anatomical lung regions, including the poorly studied distal lung areas. We also performed the first systematic quantification of tissue-infiltrating basophils in COPD-affected lungs. Finally, using an experimental model, we explored respiratory viral infections as a potential trigger of transient and patchy eosinophilia.

MATERIALS AND METHODS

Materials and methods are summarised here, further detailed procedures are provided in the online supplement.

Samples from Participants

For the main study, surgical tissues were collected from 57 patients at Skåne University Hospital in Lund, Sweden, and processed for histologic analysis. Lung resection samples were obtained from patients with mild to severe COPD (Global Initiative for Chronic Obstructive Lung Disease [GOLD] Stages I–III) and controls (never-smokers/smokers) undergoing surgery for delineated tumours). For patients with very severe (GOLD IV) COPD, lung tissue was obtained from explanted lungs after transplantation surgery. Patient demographics are presented in Table 1. Messenger ribonucleic acid (mRNA)-preserved tissues for *in-situ* hybridization (ISH) were collected from bronchial biopsies from 30 additional patients (Table E2). Tissue processing protocols were identical for all patient groups. All clinical procedures were approved by the local Swedish Research Ethics Committee in Lund, Sweden. All participants signed informed consent forms.

Immunohistochemistry

After antigen retrieval (PT-Link machine, DakoCytomation, Glostrup, Denmark), tissue sections were subjected to automated double and triple immunostaining (Autostainer Plus, DakoCytomation, Denmark). The main analysis used a triple immunohistochemistry **(**IHC) protocol to simultaneously detect eosinophils, basophils, and the Th_2 surrogate marker GATA3. Th_2 lymphocytes were identified as $GATA3^+$, $CD4^+$ cells. ILC2 cells were identified as lineage-negative, $CD25^+$, $GATA3^+$ cells after confounding non-ILC2 cells were physically blocked by

prior chromogenic staining and denaturating blocking, as we described previously [20]). Various standard IHC cell markers were also used for general immune cell exploration and for identification of chemokine-expressing cells. All antibodies had been extensively validated for use in clinical diagnosis or research (Table E1).

In-Situ Hybridization

Human and mouse eotaxin-1 (CCL11) and eotaxin-2 (CCL24) mRNA were visualised using the RNAscope 2.5 assay kit (Advanced Cell Diagnostics, Hayward, CA, USA). Sections were incubated with endogenous enzyme block, boiled in pretreatment buffer, and treated with protease prior to target probe hybridization (CCL11, CCL24). Target RNA was amplified and visualised with coloured chromogen.

Quantitative Immunohistochemistry and Computerised Image Analysis

All whole IHC- and ISH-stained sections were digitised using a ScanScope Slide Scanner (Aperio Technologies, Vista, CA, USA). High-resolution images were subjected to computerised analysis, and the immunoreactivity/detection chromogens were colour segmented, quantified, and normalized to the analyzed tissue area (Visiomorph™, Visiopharm, Denmark). For each patient in the main study, several large sections containing bronchioles, bronchi (GOLD IV only), pulmonary vessels, and alveolar parenchyma were analysed, representing two to three separated lung regions. X,Y coordinates from computer-segmented individual cells were analysed by methods for spatial distribution and cell clustering (point pattern analysis) and accumulation of GATA3 cells within defined eosinophil microenvironments (Neighbour analysis, Cell Community Viewer, CCV 1.22, Medetect, Lund, Sweden, and Monte Carlo simulation; Figure E1, online supplement).

Model of Viral Exacerbation with and without Prior Smoke Exposure

Archive lung mouse tissues [21, 22] were used to investigate potential eosinophil chemotaxis responses and formation of patchy eosinophilia in wild type or IL-33-deficient mice terminated 6 days after exposure to virus (mouse-adapted H1N1 influenza A; A/FM/1/47-MA) with or without 11 days of prior daily tobacco smoke exposure. These studies were approved by AstraZeneca/MedImmune's Institutional Animal Care and Use Committee.

Statistical Analysis

Data were analysed in GraphPad Prism (GraphPad Software). The nonparametric Kruskal-Wallis test detected overall differences between patient groups, and Dunn's test evaluated *post-hoc* between-group comparisons conservatively. The Spearman rank (rs) correlation test detected significant correlations between groups. Spatial interaction and bivariate point pattern analysis were performed by computerised point pattern generation and circular neighbourhood analysis (CCV, Medetect, Sweden), and by Monte Carlo simulation tests (ImageJ v1.51S, NIH, USA) and the MOSAIC Interaction Analysis Plugin. For mouse experiments, an unpaired *t*-test detected differences between virus-infected mouse groups. Pearson parametric correlation and linear regression determined eotaxin mRNA correlation with tissue virus content.

RESULTS

Additional results are presented in the online supplement, supplementary Tables E2, and Figures E1–4.

Samples from Participants

The main surgical tissue study included patients with COPD and controls (N=57). Demographics and clinical characteristics are presented in Tables 1 and E2.

Tissue Infiltration of Eosinophils and Basophils in COPD Occurs Across all Major Anatomical Lung Regions

Conducting airways

IHC revealed scattered bronchial eosinophils and basophils in most patients. However, more dense eosinophilia was present only in a subset of the patients and statistically increased densities compared to controls or milder disease was only found in advanced stage (GOLD IV) COPD (Figures 1–2). Basophil counts, although smaller than for eosinophils, were significantly increased in advanced stage COPD (Figure 1). Intriguingly, epithelial basophils were virtually absent in controls and mild disease, had a tendency towards increase in GOLD-II-III, and were markedly upregulated in GOLD IV patients. Similarly, densities of the type 2 surrogate marker GATA3 were increased in advanced disease (Figure 1c). Bronchi (large airways) displayed similar high eosinophil, basophil, and GATA3 levels as bronchioles from the same GOLD IV patients (Figure E2c). In the biopsy cohorts, both eosinophils and basophils were statistically increased in pooled GOLD I-III patients compared to never-smokers, but not smoking controls (Figure E2 a–b).

Distal lung compartments

Most patients had detectable eosinophil levels in the peripheral lung tissue including the alveolar parenchyma and distal lymphoid tissue. Statistically elevated eosinophil levels were observed in GOLD IV (Figure 3). Particularly high counts of eosinophils were associated with ectopic lymphoid follicles (an immunopathologic hallmark of COPD; Figures 2b and 3a) that were also rich in $GATA3^+$ cells (Figure 3c). Eosinophil counts were greater, but basophils displayed a similar magnitude of relative increased density in distal lung compartments compared with non-COPD controls (Figures 2 and 3).

Tissue eosinophilia and basophil infiltration are spatially linked

A significant statistical correlation was found between eosinophil and basophil densities within the same tissue environments, represented here by the 2–4 cm^2-size surgical resection blocks. This correlation was present in both central airways (bronchi) and distal lung compartments, such as small airways (bronchioles), the total peripheral lung tissue, and the alveolar parenchyma (Figure 4).

Accumulation of Tissue-Infiltrating Eosinophils in COPD is Patchy and Concentrated in Spatially Distinct Th_2 Microenvironments

Distinct eosinophil and basophil microenvironments in COPD lungs

We observed marked patchiness of the eosinophil distribution at a microenvironmental level (Figure 5). Eosinophils within a typical lung tissue section were commonly restricted to distinct focal microenvironments (eosinophil pockets; Figures 5a, c, E1, and E3). Enumeration of eosinophil and basophil clusters and their content of $GATA3^+$ in distal lung blocks revealed a marked cluster increase in GOLD IV COPD (Figure 5d). Spatial eosinophil and basophil clusters

were found in all anatomical lung regions, the most distinct examples being in the lamina propria region in bronchi and bronchioles (small airways; where neighbour analysis confirmed a statistically secured clustering, $p<0.001$).

Eosinophil microenvironment is linked to a localised GATA3 signature

Repeated staining further revealed that the presence of distinct eosinophil-rich microenvironments was accompanied by focal gathering of basophils and $GATA3^+$ cells (Figure 5a,c). A spatial statistics analysis approach was used to quantify the density of $GATA3^+$ cells inside and outside the eosinophil microenvironments (Figure E1). For lung samples with patchy eosinophilia, the density and clustering of $GATA3^+$ cells was significantly and several-fold greater in eosinophil neighbourhood microenvironments compared with non-neighbourhood regions (Figure 5b). A spatial GATA3-eosinophil relationship was also confirmed by point pattern Monte Carlo simulations ($p<0.001$).

Presence of type 2 innate lymphoid cells and Th_2 lymphocytes in eosinophil microenvironments

ILC2 cells could represent a local type 2 cytokine source, promoting the present type of localised eosinophilia. Our unique ILC2 staining protocol showed clear localization of ILC2 cells within eosinophil foci (Figure 6a). As expected, ILC2 counts were significantly lower than for classic $CD4^+$ Th_2 lymphocytes with the ILC2 fraction of the sum of ILC2 and Th_2 cells in eosinophil-rich patients being 3.5 ± 3.8% (mean ± SD). Notably, the fraction of ILC2 cells in the airway epithelium was 15.5 ± 18% (mean ± SD) of the sum of ILC2 and Th_2 cells.

Exploration of Respiratory Viral Infections as a Potential Cause of Patchy and Spatially Distinct Eosinophil Accumulation in Lung Tissues

Our results, from exploration of eosinophil responses in lung tissues from a validated mouse exacerbation model with smoke and/or influenza infection, demonstrate that viral infection causes a robust infiltration of eosinophils (Figures 7a and E4d). The generated eosinophilia was patchy and co-localised to the patchy infection (influenza presence) described in the present model (Figure 7) [21]. Mice exposed to prior tobacco smoke did not mount a similar eosinophil response upon infection (Figure 7). The development of influenza-induced eosinophilia seems to involve mediators of the IL-33/ST2 axis, as virus-induced eosinophilia did not develop in IL-$33^{-/-}$ mice (Figure 7a, left). The knockout of IL-33 in itself significantly reduced the low-grade baseline presence of eosinophils in noninfected wild-type mice (Figure 7a, right).

COPD-Affected Lungs and Virus-Infected Mice Display Localised Expression of Eotaxins

Eotaxins are key chemoattractants for the migration and tissue homing of eosinophils. Combined ISH+IHC was used to reveal the presence and identity of eotaxin-expressing cells in patients with COPD and virus-infected mice. Virus infection in mice elicited strong and significant upregulation of both total lung CCL11 and CCL24 (Figure 7b). The expression for CCL11 was distinct, restricted to large perivascular structural cells (Figure 7c and 7d), and primarily localized to infected and eosinophil-rich lung areas (Figure 7c and 7d). The distribution of CCL24 was more widespread than CCL11 and foremost localised to alveolar macrophages within infected and eosinophil-rich lung areas (Figure E4c).

In human COPD tissues, CCL11 had a variable and patchy localization and was expressed by a subset of elongated fibroblast-like (vimentin^{+}) structural cells. In contrast to mice, CCL11 in

human COPD-affected lungs was localised mainly just under the airway or glandular epithelium (Figure 6b), which was also the most prominent site for eosinophil clusters. CCL24-expressing cells were mainly $CD68^{+}$ alveolar macrophages (Figure 6c) and had no visually apparent co-localisation to eosinophil clusters.

DISCUSSION

This study reveals several new aspects of eosinophils, basophils, and Th_2 immunity in COPD, particularly the lack of inflammation uniformity in COPD-affected lungs. The study excluded patients with any atopy or history of allergy. Therefore, the data reveal the nature of COPD-specific eosinophilia and Th_2 immunity for the type of eosinophilia currently under intense investigation in COPD and nonallergic asthma phenotypes. Interestingly, eosinophil-high COPD has been demonstrated to display histopathologic features normally ascribed to eosinophilic asthma, such as thickening of the reticular layer of the basement membrane [23]. This raises the possibility of shared underlying type 2 mechanisms. Therefore, although we are confident about the diagnosis of COPD in this study, we acknowledge the complexity related to its definition and the differential diagnosis between nonallergic eosinophilic asthma with fixed obstruction, eosinophil-high COPD, and asthma-COPD overlap syndrome (ACOS) [24].

The fact that elevated eosinophil and basophil numbers were observed for patients with COPD with very severe disease receiving high-dosage inhaled corticosteroid treatment further supports observations in asthma that nonallergic eosinophilia is more resistant to steroids than classic allergen-induced eosinophilia. This also agrees with reports that alveolar nitric oxide concentration is increased in patients with more advanced COPD, indicating an increased nonallergic type 2 signal in the distal airways [25]. The issue of steroid sensitivity for patients with COPD is complicated by observations of blood or sputum eosinophilia in milder disease being an indicator of increased responsiveness [26, 27]. Notably, in our sub-biopsy study, both eosinophils and basophils were also increased in milder disease. Because there was no perfect age and gender match with control patients, however, this result should be interpreted with caution,

and it should be noted that the sample size of our study does not permit any conclusion about steroid responsiveness.

Previous studies have found eosinophilia to be a significant feature in a subset of COPD patients [6]. In the present study, a statistical increase in eosinophilia was detected only in very severe COPD. It should be noted that all GOLD IV patients had ceased smoking whereas around 40% of the milder patients were current smokers. Hence, because smoke exposure can counteract type 2 responses (which was here supported by the present mouse experiments), it cannot be excluded that ongoing smoking may contribute to the lower eosinophilia observed in milder disease. Furthermore, the present study design cannot inform to what degree transient eosinophilia occurs in exacerbating GOLD I–III patients. A novel study finding was the anatomically widespread eosinophil infiltration involving all major anatomical compartments in COPD-affected lungs. The results complement another study reporting that patients with COPD and greater blood eosinophil counts (>250 cells/μL) had correspondingly greater sputum and bronchoalveolar lavage eosinophil counts compared with patients with lesser blood eosinophil counts (<150 cells/μL) [28]. These patients with eosinophilic COPD also had increased eosinophils in various lung locations and greater tissue remodelling [28]. Apart from the previously identified luminal and bronchial eosinophilia in nonallergic patients with COPD [9, 29, 30], eosinophils in COPD may exert effector functions in bronchioles, the alveolar parenchyma, and ectopic lymphoid aggregates.

Another major observation was that the distribution of eosinophils displayed a marked and distinct patchiness at a microenvironmental level. This indicates that the underlying, but unidentified, cause of eosinophilia in nonallergic patients with COPD is likely to emanate from

external sources that act in a highly localised fashion. It also means that the immunologic responses eliciting and manifesting eosinophilia are probably also highly localised. This was supported by our finding of a clear spatial relationship between eosinophils and the surrogate type 2 marker GATA3. Expression of GATA3 is essential for type 2 cytokine-production by both Th2 lymphocytes and ILC2 cells [31–33] and is targeted to combat type 2 immunity in the clinic [30]. Therefore, it was important to find that not only $GATA3^+$ Th_2 lymphocytes but also $GATA3^+$ ILC2 cells were identified in eosinophil-rich pockets. ILC2 cells with capacity to produce type 2 cytokines have previously been demonstrated in COPD lungs in small (approximately 0.05% of the $CD45^+$ cells) but most likely biologically relevant numbers [34]. In agreement, our study revealed a clear dominance of Th2 cells over ILC2s in numbers, although the ILC2/Th2 ratio was only approximately 1:6 in the epithelium lining.

Our finding of highly localised Th_2 and eosinophil-rich pockets in COPD-affected lungs is conceptually novel, and an important future challenge for evaluating patients' inflammatory status. For example, blood or sputum eosinophilia indicates the presence of tissue eosinophilia but does not exclude the possibility that a significant portion or other lung regions will have an innate macrophage and neutrophil-rich, or Th_1, type inflammation. This represents a significant future challenge for improved personalized treatment and helps to understand the challenges of targeting type 2 mechanisms in COPD lungs.

In agreement with published studies in human and mice showing that viral infections can evoke a transient eosinophilia [35–37], this study confirms that robust eosinophilia develops after an influenza infection in mouse lungs. In our experimental model we reveal further that this eosinophil response is highly patchy, associated with a spatially localized eotaxin response, and

dependent on IL-33 release, as eosinophilia did not develop in IL-33$^{-/-}$ mice. In addition, in agreement with experimental myocarditis models [38], our combined ISH and IHC revealed CCL11 to be foremost expressed by fibroblasts and pericytes whereas CCL24 was localized in macrophages. Our experimental data, along with the fact that viral infections are common during COPD exacerbations [39], propose patchy localised infections as one plausible trigger of the present novel type of patchy type 2, eosinophil-rich pockets. Indeed, our data suggest that patchy eosinophilia is more common in advanced disease, during which patients develop more infections compared with earlier stages [39]. However, a limitation of our study was that patient groups were relatively small, and the evidence for an infectious cause of patchy eosinophilia remains indirect. Larger studies that involve larger cohorts and broader assessment of microbes (bacteria and viruses) are thus warranted.

This study also represents the first systematic mapping of tissue-infiltrating basophils in COPD. Altogether, the basophil densities correlated with that of eosinophils. However, because basophils are virtually absent under controlled situations, the relative magnitude of increase was larger than is usually observed for many other immune cells. Interestingly, similar to observations for asthma [40], the tissue density of basophils increased with disease severity. The preferential sites of infiltration were ectopic lymphoid tissue in distal lung and conducting airways, where, for example, intraepithelial basophils in small airways displayed a dramatic increase in GOLD IV patients. This infiltration pattern is compatible with the modern view of basophils as potent immune modulators and host defence cells [41, 42]. For example, basophils may amplify a localised type 2 response by IL-4 secretions [11, 43], are activated by IL-33 and thymic stromal lymphopoietin, and may release a variety of proinflammatory cytokines in addition to histamine. In recent experimental models, basophils have been identified as having a role in emphysema

development [44] and they have also been linked to the defence against COPD-relevant bacteria and viruses [41]. Basophils may thus, beside their harmful pathogenic capacity, also play a protective role. In any case, the present study suggests that basophils, which like eosinophils express IL-5Rα, should be recognised as a potentially relevant target for IL-5- and IL-5Rα-targeting therapies.

It remains to be explored to what extent eosinophils in COPD tissues undergo piecemeal degranulation, programmed cytolysis, or secondary necrosis [43, 45]. Elevated free granule protein in bronchoalveolar lavage fluid or sputum samples in asthma and COPD has frequently been viewed as a sign of active degranulation [46], but liberation of luminal granule proteins is noticeably caused by intraluminal necrotic mechanisms. Unfortunately, our samples were not suitable for electron microscopy, preventing an ultrastructural analysis of degranulation status, and the activation status of eosinophils in COPD tissues also remains to be determined.

In summary, this study identifies basophils as having a potential role in COPD and demonstrates that tissue eosinophilia in COPD is anatomically widespread but commonly confined to distinct Th_2-skewed and ILC2-containing microenvironments. This feature of tissue eosinophilia is likely to have clinical implications. Our data also suggest respiratory infections as a potential trigger of patchy eosinophilia in COPD.

ACKNOWLEDGMENTS

We thank Karin Jansner, Medetect AB, Lund, and Britt-Marie Nilsson, Unit of Airway inflammation, Lund University, for skilful tissue preparation and histologic work. Editing support, under the direction and guidance of the authors, and manuscript submission, was provided by Debra Scates, PhD, of JK Associates, Inc. (Conshohocken, PA, USA), and Michael A. Nissen, ELS, of AstraZeneca (Gaithersburg, MD, USA). This support was funded by AstraZeneca.

DISCLOSURES

Jennifer Kearley and Paul Newbold are employees of AstraZeneca (previously MedImmune LLC) and have received stock options from AstraZeneca. Alison A. Humbles and Roland Kolbeck were employees of AstraZeneca (previously MedImmune LLC) at the time these analyses were conducted. Jonas S. Erjefält, is founder (and stock owner) of Medetect AB who received funding from AstraZeneca for conducting parts of the present study. Leif Bjermer, Prajakta Jogdand, Premkumar Siddhuraj, Jimmie Jönsson, Michiko Mori, Caroline Sanden and Andrew F. Walls have nothing to declare.

FINANCIAL SUPPORT

Funding for this study was provided by AstraZeneca, the Swedish Heart and Lung Foundation, and the Swedish Research Council.

REFERENCES

1. Rabe KF, Hurd S, Anzueto A, et al. Global strategy for the diagnosis, management, and prevention of chronic obstructive pulmonary disease: GOLD executive summary. *Am J Respir Crit Care Med* 2007; 176: 532–555.
2. Hogg JC, Timens W. The pathology of chronic obstructive pulmonary disease. *Annu Rev Pathol* 2009; 4: 435–459.
3. Barnes PJ. Immunology of asthma and chronic obstructive pulmonary disease. *Nat Rev Immuno*l 2008; 8: 183–192.
4. Mori M, Andersson CK, Svedberg KA, et al. Appearance of remodelled and dendritic cell-rich alveolar-lymphoid interfaces provides a structural basis for increased alveolar antigen uptake in chronic obstructive pulmonary disease. *Thorax* 2013; 68: 521–531.
5. Hogg JC, Chu F, Utokaparch S, et al. The nature of small-airway obstruction in chronic obstructive pulmonary disease. *New Engl J Med* 2004; 350: 2645–2653.
6. George L, Brightling CE. Eosinophilic airway inflammation: role in asthma and chronic obstructive pulmonary disease. *Ther Adv Chronic Dis* 2016; 7: 34–51.
7. Singh D, Kolsum U, Brightling CE, et al. Eosinophilic inflammation in COPD: prevalence and clinical characteristics. *Eur Respir J* 2014; 44: 1697–1700.
8. Vedel-Krogh S, Nielsen SF, Lange P, et al. Blood eosinophils and exacerbations in chronic obstructive pulmonary disease. The Copenhagen General Population Study. *Am J Resp Crit Care* 2016; 193: 965–974.
9. Bafadhel M, McKenna S, Terry S, et al. Acute exacerbations of chronic obstructive pulmonary disease: identification of biologic clusters and their biomarkers. *Am J Resp Crit Care* 2011; 184: 662–671.

10. Willebrand R, Voehringer D. Regulation of eosinophil development and survival. *Curr Opin Hematol* 2017; 24: 9–15.

11. Wynn TA. Type 2 cytokines: mechanisms and therapeutic strategies. *Nat Rev Immunol* 2015; 15: 271–282.

12. Brightling CE, Bleecker ER, Panettieri RA, et al. Benralizumab for chronic obstructive pulmonary disease and sputum eosinophilia: a randomised, double-blind, placebo-controlled, phase 2a study. *Lancet Resp Med* 2014; 2: 891–901.

13. Pavord ID, Chanez P, Criner GJ, et al. Mepolizumab for eosinophilic chronic obstructive pulmonary disease. *N Engl J Med* 2017; 377: 1613–1629.

14. Sridhar S, Liu H, Pham TH, Damera G, Newbold P. Modulation of blood inflammatory markers by benralizumab in patients with eosinophilic airway diseases. *Respir Res* 2019; 20: 14.

15. Lacoste JY, Bousquet J, Chanez P, et al. Eosinophilic and neutrophilic inflammation in asthma, chronic bronchitis, and chronic obstructive pulmonary disease. *J Allergy Clin Immunol* 1993; 92: 537–548.

16. Turato G, Semenzato U, Bazzan E, et al. Blood eosinophilia neither reflects tissue eosinophils nor worsens clinical outcomes in chronic obstructive pulmonary disease. *Am J Respir Crit Care Med* 2018; 197: 1216–1219.

17. Walker JA, Barlow JL, McKenzie AN. Innate lymphoid cells--how did we miss them? *Nat Rev Immunol* 2013; 13: 75–87.

18. Spits H, Cupedo T. Innate lymphoid cells: emerging insights in development, lineage relationships, and function. *Annu Rev Immunol* 2012; 30: 647–675.

19. Brusselle GG, Joos GF, Bracke KR. New insights into the immunology of chronic obstructive pulmonary disease. *Lancet* 2011; 378: 1015–1026.

20. Bal SM, Bernink JH, Nagasawa M, et al. IL-1β, IL-4 and IL-12 control the fate of group 2 innate lymphoid cells in human airway inflammation in the lungs. *Nat Immunol* 2016; 17: 36–45.

21. Silver JS, Kearley J, Copenhaver AM, et al. Inflammatory triggers associated with exacerbations of COPD orchestrate plasticity of group 2 innate lymphoid cells in the lungs. *Nat Immunol* 2016; 17: 626–635.

22. Kearley J, Silver JS, Sanden C, et al. Cigarette smoke silences innate lymphoid cell function and facilitates an exacerbated type I interleukin-33-dependent response to infection. *Immunity* 2015; 42: 566–579.

23. Eltboli O, Mistry V, Barker B, et al. Relationship between blood and bronchial submucosal eosinophilia and reticular basement membrane thickening in chronic obstructive pulmonary disease. *Respirology* 2015; 20: 667–670.

24. Woodruff PG, van den Berge M, Boucher RC, et al. American Thoracic Society/National Heart, Lung, and Blood Institute Asthma-Chronic Obstructive Pulmonary Disease Overlap Workshop Report. *Am J Respir Crit Care Med* 2017; 196: 375–381.

25. Brindicci C, Ito K, Resta O, et al. Exhaled nitric oxide from lung periphery is increased in COPD. *Eur Respir J* 2005; 26: 52–59.

26. Bafadhel M, McKenna S, Terry S, et al. Blood eosinophils to direct corticosteroid treatment of exacerbations of chronic obstructive pulmonary disease: a randomized placebo-controlled trial. *Am J Respir Crit Care Med* 2012; 186: 48–55.

27. Bafadehl M, Peterson S, De Blas MA, et al. Predictors of exacerbation risk and response to budesonide in patients with chronic obstructive pulmonary disease: a post-hoc analysis of three randomised trials. *Lancet Respir Med* 2018; 6: 117–126.

28. Kolsum U, Damera G, Pham T-H, et al. Pulmonary inflammation in patients with chronic obstructive pulmonary disease with higher blood eosinophil counts. *J Allergy Clin Immunol* 2017; 140: 1181–1184.e7

29. Snoeck-Stroband JB, Lapperre TS, et al. Chronic bronchitis sub-phenotype within COPD: inflammation in sputum and biopsies. *Eur Resp J* 2008; 31: 70–77.

30. Nair P, Ochkur SI, Protheroe C, et al. Eosinophil peroxidase in sputum represents a unique biomarker of airway eosinophilia. *Allergy* 2013; 68: 1177–1184.

31. Das J, Chen CH, Yang L, Cohn L, Ray P, Ray Aet al. A critical role for NF-kappa B in GATA3 expression and TH2 differentiation in allergic airway inflammation. *Nat Immunol* 2001; 2: 45–50.

32. Nakayama T, Hirahara K, Onodera A, *Endo Y, Hosokawa H, Shinoda K, Tumes DJ, Okamoto Yet al*. Th2 Cells in Health and Disease. *Annu Rev Immunol* 2016; 35: 53–84.

33. Klein Wolterink RG, Serafini N, van Nimwegen M, et al. Essential, dose-dependent role for the transcription factor Gata3 in the development of IL-5+ and IL-13+ type 2 innate lymphoid cells. *Proc Natl Acad Sci U.S.A.* 2013; 110: 10240–10245.

34. De Grove KC, Provoost S, Verhamme FM, et al. Characterization and quantification of innate lymphoid cell subsets in human lung. *PLoS One* 2016; 11: e0145961.

35. Su YC, Townsend D, Herrero LJ, et al. Dual proinflammatory and antiviral properties of pulmonary eosinophils in respiratory syncytial virus vaccine-enhanced disease. *J Virol* 2015; 89: 1564–1578.

36. Samarasinghe AE, Melo RC, Duan S, et al. Eosinophils promote antiviral immunity in mice infected with influenza A virus. *J Immunol* 2017; 198: 3214–3226.

37. Fraenkel DJ, Bardin PG, Sanderson G, Lampe F, Johnston SL, Holgate ST. Lower airways inflammation during rhinovirus colds in normal and asthmatic subjects. *Am J Respir Crit Care Med* 1995; 151: 879–886.

38. Diny NL, Hou X, Barin JG, et al. Macrophages and cardiac fibroblasts are the main producers of eotaxins and regulate eosinophil trafficking to the heart. *Eur J Immunol* 2016; 46: 2749–2760.

39. Sethi S, Mallia P, Johnston SL. New paradigms in the pathogenesis of chronic obstructive pulmonary disease II. *Proc Am Thorac Soc* 2009; 6: 532–534.

40. Kepley CL, McFeeley PJ, Oliver JM, et al. Immunohistochemical detection of human basophils in postmortem cases of fatal asthma. *Am J Respir Crit Care Med* 2001; 164: 1053–1058.

41. Karasuyama H, Yamanishi Y. Basophils have emerged as a key player in immunity. *Curr Opin Immunol* 2014; 31: 1–7.

42. Wedemeyer J, Tsai M, Galli SJ. Roles of mast cells and basophils in innate and acquired immunity. *Curr Opin Immunol* 2000; 12: 624–631.

43. Erjefalt JS, Persson CG. New aspects of degranulation and fates of airway mucosal eosinophils. *Am J Respir Crit Care Med* 2000; 161: 2074–2085.

44. Shibata S, Miyake K, Tateishi T, et al. Basophils trigger emphysema development in a murine model of COPD through IL-4-mediated generation of MMP-12-producing macrophages. *Proc Natl Acad Sci* 2018; 115: 13057–13062.

45. Melo RC, Weller PF. Piecemeal degranulation in human eosinophils: a distinct secretion mechanism underlying inflammatory responses. *Histol Histopathol* 2010; 25: 1341–1354.

46. Adelroth E, Rosenhall L, Johansson SA, et al. Inflammatory cells and eosinophilic activity in asthmatics investigated by bronchoalveolar lavage. The effects of antiasthmatic treatment with budesonide or terbutaline. *Am Rev Respir Dis* 1990; 142: 91–99.

Table 1. Patient Demographics

Parameters	**Never-smokers**	**Smokers w/o COPD**	**GOLD Stage I COPD**	**GOLD Stage II–III[#] COPD**	**GOLD Stage IV COPD**	**Overall P-Value**
Patients[¶]	8[¶]	9	7[¶]	18[¶]	15[¶]	
Sex, male/female[¶]	2/6[¶]	3/6[¶]	4/3[¶]	13/5[¶]	5/10[¶]	
Age, years	66 (33–76)	58 (47–68)	69 (56–75)	70 (53–75)[§]	62 (53-66)[*f*]	0.015
Height, m	1.6 (1.5–1.8)	1.7 (1.6–1.8)	1.7 (1.6–1.8)	1.7 (1.5–1.9)	1.7 (1.5–1.9)	0.276
Body mass index, kg/m^2	22.6 (19.8–29.7)	23.4 (19.7–28.3)	23.8 (20.3–28.4)	25.2 (17.7–34.1)	23.6 (17.0–31.2)	0.807
Smoking history, pack-years	0	36 (15–80)	46 (25–66) ¤	46 (30–65) [##]	40 (20–60) ¤	<0.001
Smoking status, ex-smokers/current	NA	5/4	3/4	12/5[&]	15/0	
FEV_1, L	2.5 (1.7–5.1)	2.67 (1.8–3.5)	2.8 (1.6–3.2)	1.9 (1.1–2.9)	0.6 (0.36–1.0) [##] ¶¶++ &&	<0.0001

FEV_1/FVC, %	81.5 (66–121)	76 (71–88)	66.5 (65–70)	61.5 (41–70) §§¤¤	32 (20–39)*f* ## ¶¶*fff*	<0.0001
FEV_1, % predicted	108 (82–141)	95 (75–120)	86.66 (80–95)	69 (43.2–77.8) ¤,¤¤	23.84 (15–28) ##¶¶++*f*	<0.0001
Inhaled β_2-agonists						
Short-acting, yes/no/unknown	0/8/0	0/9/0	2/5/0	4/11/3	9/5/1+	
Long-acting, yes/no/unknown	0/8/0	0/9/0	1/6/0	2/13/3	6/8/1+	
Inhaled anticholinergics						
Short-acting, yes/no/unknown	0/8/0	0/9/0	1/6/0	3/12/3	6/8/1+	
Long-acting, yes/no/unknown	0/8/0	0/9/0	0/7/0	2/13/3	10/4/1+	
Inhaled short-acting β_2-agonist plus anticholinergics,	0/8/0	0/9/0	0/7/0	1/14/3	3/11/1+	

yes/no/unknown						
Corticosteroids Inhaled, yes/no/unknown Oral, yes/no/unknown	0/8/0 0/8/0	0/9/0 0/9/0	0/7/0 0/7/0	2/13/3 0/15/3	2/12/1[+] 2/12/1[+]	
Inhaled long-acting β_2-agonist plus corticosteroids, yes/no/unknown	0/8/0	0/9/0	0/7/0	2/13/3	9/4/2[+]	
Mucolytics, yes/no/unknown	0/8/0	0/9/0	2/5/0	0/15/3	7/6/2[+]	

COPD, chronic obstructive pulmonary disease; FEV_1, forced expiratory volume in 1 second; FVC, forced vital capacity; GOLD, Global Initiative for Chronic Obstructive Lung Disease; NA, not applicable. Values are median (range) or n. Statistical analysis was performed using Kruskal-Wallis nonparametric test followed by Dunn's multiple comparison post-test. [#]Two patients with GOLD Stage III COPD (median value of FEV_1 % of predicted, 44.5%; range 43.2–45.9). [¶]The mean value of the study group is 64 years. [+]One patient with unknown medical history. [&]Data from one patient is missing. [##]$p<0.0001$ vs. never-smokers. [§§]$p<0.01$ vs. never-smokers. ¤$p<0.005$ vs

never-smokers. [§]p<0.01 vs. smokers without COPD. ¤¤p<0.05 vs. smokers without COPD, [¶¶]p<0.0001 vs. smokers without COPD. [++]p<0.0005 vs. patients with GOLD Stage I COPD. [ƒƒ]p<0.05 vs. patients with GOLD Stage I COPD. [ƒƒƒ]p<0.02 vs. patients with GOLD Stage I COPD. [ƒ]p<0.05 vs. patients with GOLD Stage II–III COPD. [&&]p<0.005 vs patients with GOLD Stage II–III COPD. For further patient description, including inclusion and exclusion criteria, see the online supplement data.

FIGURE LEGENDS

Figure 1. (a–c) Scattergrams showing densities of tissue-infiltrating eosinophils and basophils and the surrogate type 2 immune marker GATA3 in the total wall, epithelial, and subepithelial compartments of bronchioles [small airways] in patients with GOLD I–IV COPD and matching controls. Dots and horizontal dashes represent patient mean densities and group median values, respectively. Asterisks denote degrees of statistical significance between groups: *$p<0.05$, **$p<0.01$, ***$p<0.001$. P-values quoted in the figure represent overall statistical difference between patients with COPD and controls, as determined by a nonparametric Kruskal-Wallis one-way ANOVA with Dunn's multiple comparison *post-hoc* test (mean rank of each subgroup is compared to every other subgroup).

COPD, chronic obstructive pulmonary disease; GOLD, Global Initiative for Chronic Obstructive Lung Disease.

Figure 2. Bright field micrographs exemplifying eosinophil, basophil, and GATA3 staining in patients with COPD representative of an eosinophil-high profile. (a and b) Single eosinophil staining (brown EG2 immunoreactivity). (c) Double IHC lung section stained for basophils (red, AP) and eosinophils (vina green). (d) Triple IHC staining for eosinophils (vina green), basophils (red, AP), and GATA3 (brown DAB; inset in d exemplifies greater magnification of triple-stained section and brown $GATA3^+$ cells amid green $EG2^+$ eosinophils and a red $BB1^+$ basophil). Arrows or arrowheads in c and d point to positive cells.

Alv, alveolar parenchyma; Baso, basophil; COPD, chronic obstructive pulmonary disease; Eos, eosinophil; IHC, immunohistochemistry; LA, lymphoid aggregate; SA, small airway; AP,

alkaline phosphatase; DAB, diaminobenzidine. Scale bars: a=100 μm; b=120 μm; c=85 μm; d=50 μm.

Figure 3. (a–c) Scattergrams of densities of tissue-infiltrating eosinophils and basophils and the surrogate Th_2 marker GATA3 in distal lung compartments, here divided into total peripheral lung tissue (i.e., lung tissue in which any large conducting airways and large pulmonary vessels have been excluded), alveolar parenchyma (with small airways and large-mid-size vessels and lymphoid tissue excluded) and lymphoid-associated tissue. Dots and horizontal dashes represent patient mean densities and group median values, respectively. Asterisks denote degrees of statistical significance between groups: *$p<0.05$, **$p<0.01$, ***$p<0.001$. P-values quoted in the figure represent overall statistical difference between patients with COPD and controls, as determined by a nonparametric Kruskal-Wallis one-way ANOVA with Dunn's multiple comparison *post-hoc* test (mean rank of each subgroup is compared to every other subgroup). GOLD, Global Initiative for Chronic Obstructive Lung Disease.

Figure 4. (a–d) Scattergrams showing correlations between eosinophils and basophils in lung compartments. Individual dots are color-coded according to patient category and denote mean values in individual tissue blocks (i.e., blocks representing distinct and spatially separated anatomic regions within each analysed type of lung compartment). Values were log-transformed to yield better visualization of the correlation (as a result sections with zero values for any of the cell type are omitted). Whereas panels a–c represent surgical cases from the main study, panel d represents pooled mean values from surgical GOLD IV COPD samples and endobronchial biopsies from GOLD I–II patients collected to yield mRNA-preserved tissue samples for

chemokine mRNA visualization by *in-situ* hybridization. Spearman rank (rs) correlation test was used to determine the degree of correlation.

GOLD, Global Initiative for Chronic Obstructive Lung Disease.

Figure 5. Heterogeneous spatial distribution and presence of distinct eosinophil-rich type 2 skewed microenvironments in COPD lungs. (a) Spatially linked heat maps exemplifying a gross codistribution of $EG2^+$ eosinophils, $BB1^+$ basophils and GATA3 and depicting individual 300 x 300 μm microenvironments color-coded for cell density (black-bright represents low-high density). (b) Spatial statistics analysis (see Supplemental Figure E1 and text for methodology details) shows the quotient of GATA3 densities inside eosinophil neighbourhoods over GATA3 densities outside eosinophil neighbourhoods. Data are shown for 3 levels of computer-created circular eosinophil neighbourhoods/microenvironments, defined by a radius of 10, 20, and 40 μm around individual eosinophils, respectively. (c) Distinct spatial foci of eosinophils (pseudo color-coded red after computerised image analysis) and GATA3 (green). The clustering of eosinophils was also confirmed by point pattern statistics, nearest neighbour's distance analysis, and Ripley´s K point pattern analysis (see online supplement). (d) Quantitative data on tissue density of eosinophil clusters and/or basophil clusters, with and without content of any GATA3 cells. Dots and horizontal dashes represent patient mean clusters/mm^2 lung tissue and group median values, respectively. Asterisks denote degrees of statistical significance between groups: *$p<0.05$, **$p<0.01$, ***$p<0.001$. P-values quoted in the figure represent overall statistical difference between patients with COPD and controls, as determined by a nonparametric Kruskal-Wallis one-way ANOVA with Dunn's multiple comparison *post-hoc* test (mean rank of each subgroup is compared to every other subgroup). EOS, eosinophils; gln, subepithelial gland; LA, lymphoid aggregate; SA, small airway; sm, smooth muscle. Scale bars: a=1 cm; b=150 μm; c=250 μm.

Figure 6. (a) Example of a bronchiolar eosinophil (red) foci and presence of lineage-negative $GATA3^{+}CD25^{+}$ ILC2 cells in a GOLD IV patient, here color-coded green; cell nuclei in blue. Inserts depict the original micrographs of the same ILC2s (GATA3 in brown; CD25 in green). (b) Bright field images exemplifying focal distribution of CCL-11 (eotaxin 1) mRNA expression. CCL-11 mRNA was detected by ISH and visualised by permanent red substrate chromogen. The low power overview illustrates patchy clustering of $CCL\text{-}11^{+}$ cells, whereas greater magnification (inset in b) reveals the elongated fibroblast-like morphology of the $CCL\text{-}11^{+}$ cells. (c) Example of CD68-negative $CCL11^{+}$ (green only) cells and $CD68^{+}$ $CCL24^{+}$ (red and green) cells in a COPD-affected lung.

COPD, chronic obstructive pulmonary disease; ep, airway epithelium; GL, subepithelial mucus glands; ISH, *in-situ* hybridisation; mRNA, messenger ribonucleic acid; SA, small airway (i.e., bronchioles). Scale bars: a=100 μm (inset 10 μm); b=200 μm; c=50 μm.

Figure 7. An influenza viral infection triggers a patchy eosinophilia and a highly localised induction of pro-eosinophilic chemokines. (a, left) Infection-induced eosinophilia. Data are presented for wild-type and IL-33 knockout mice at 6 days post–influenza A infection with and without 11 days of daily tobacco smoke exposure. (a, right) Noninfected baseline counts (no virus) of eosinophils in ambient air and tobacco smoke–exposed controls. Data are presented for wild-type and IL-33 knockout mice. (b) Mean measurements of lung tissue CCL11 (left) and CCL24 (right) immunoreactivity in control and virus-infected wild-type mice at 6 days post-infection. (c and d) Spatially localised presence of CCL11 in mouse lungs at 6 days post-infection. Example of typical and highly localised CCL11 clusters (brown) in virus-infected areas (virus is stained by vina green chromogen). Note the distinct CCL11 localization around

bronchial- and bronchiole-associated pulmonary BV. Inset in d exemplifies perivascular $CCL11^{+}$ cells as well as a typical solitary CCL24+ alveolar cell.

BV, blood vessel; Br, bronchi; ISH, *in-situ* hybridization; KO, knockout; mRNA, messenger ribonucleic acid; sm, smooth muscle; WT, wild-type. Scale bars: c=200 μm; d=100 μm (inset 50 μm).

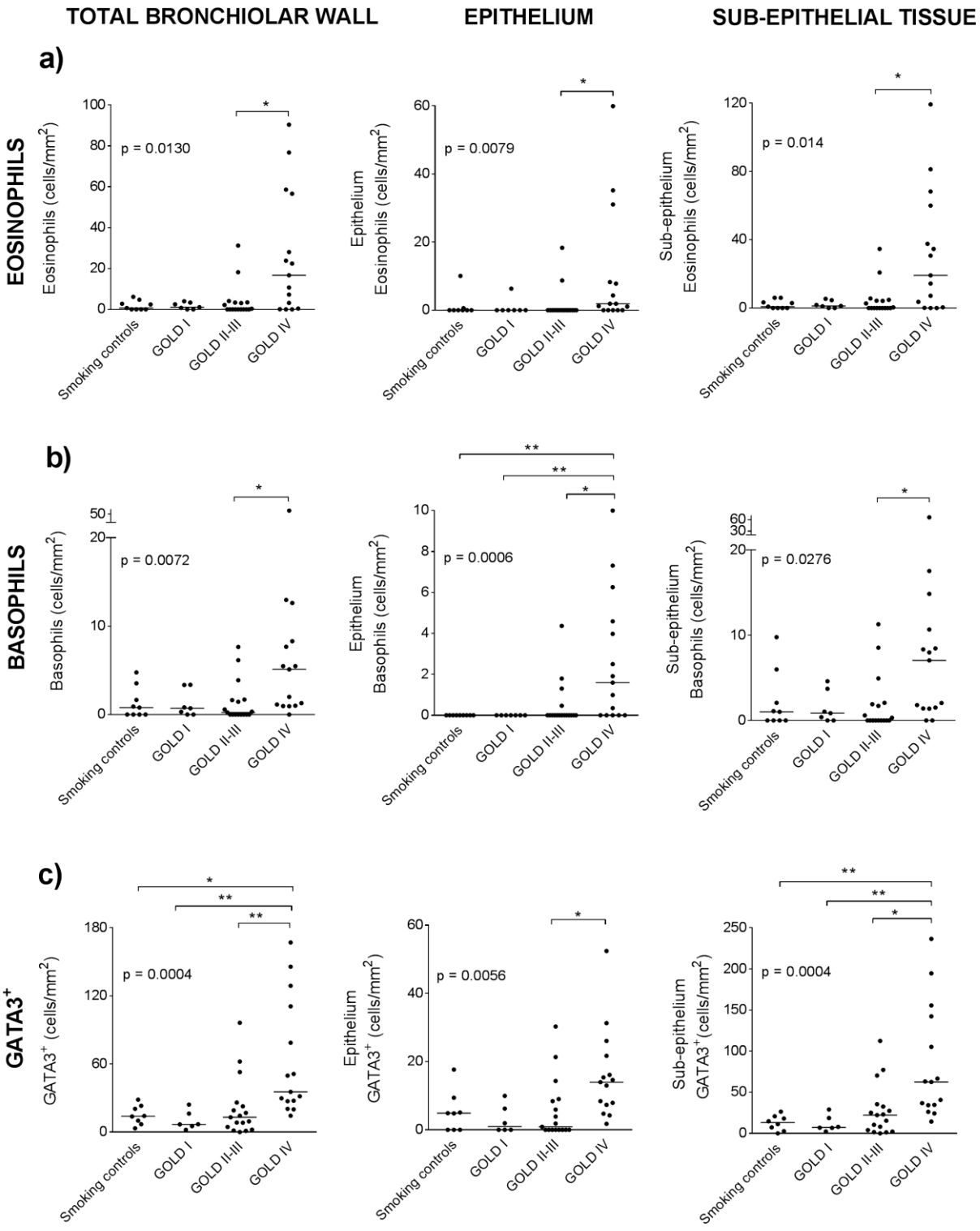
TOTAL BRONCHIOLAR WALL
EPITHELIUM
SUB-EPITHELIAL TISSUE
a)
EOSINOPHILS
Eosinophils (cells/mm2)
Epithelium Eosinophils (cells/mm2)
Sub-epithelium Eosinophils (cells/mm2)
p = 0.0130
p = 0.0079
p = 0.014
b)
BASOPHILS
Basophils (cells/mm2)
Epithelium Basophils (cells/mm2)
Sub-epithelium Basophils (cells/mm2)
p = 0.0072
p = 0.0006
p = 0.0276
c)
GATA3+
GATA3+ (cells/mm2)
Epithelium GATA3+ (cells/mm2)
Sub-epithelium GATA3+ (cells/mm2)
p = 0.0004
p = 0.0056
p = 0.0004
Smoking controls
GOLD I
GOLD II-III
GOLD IV

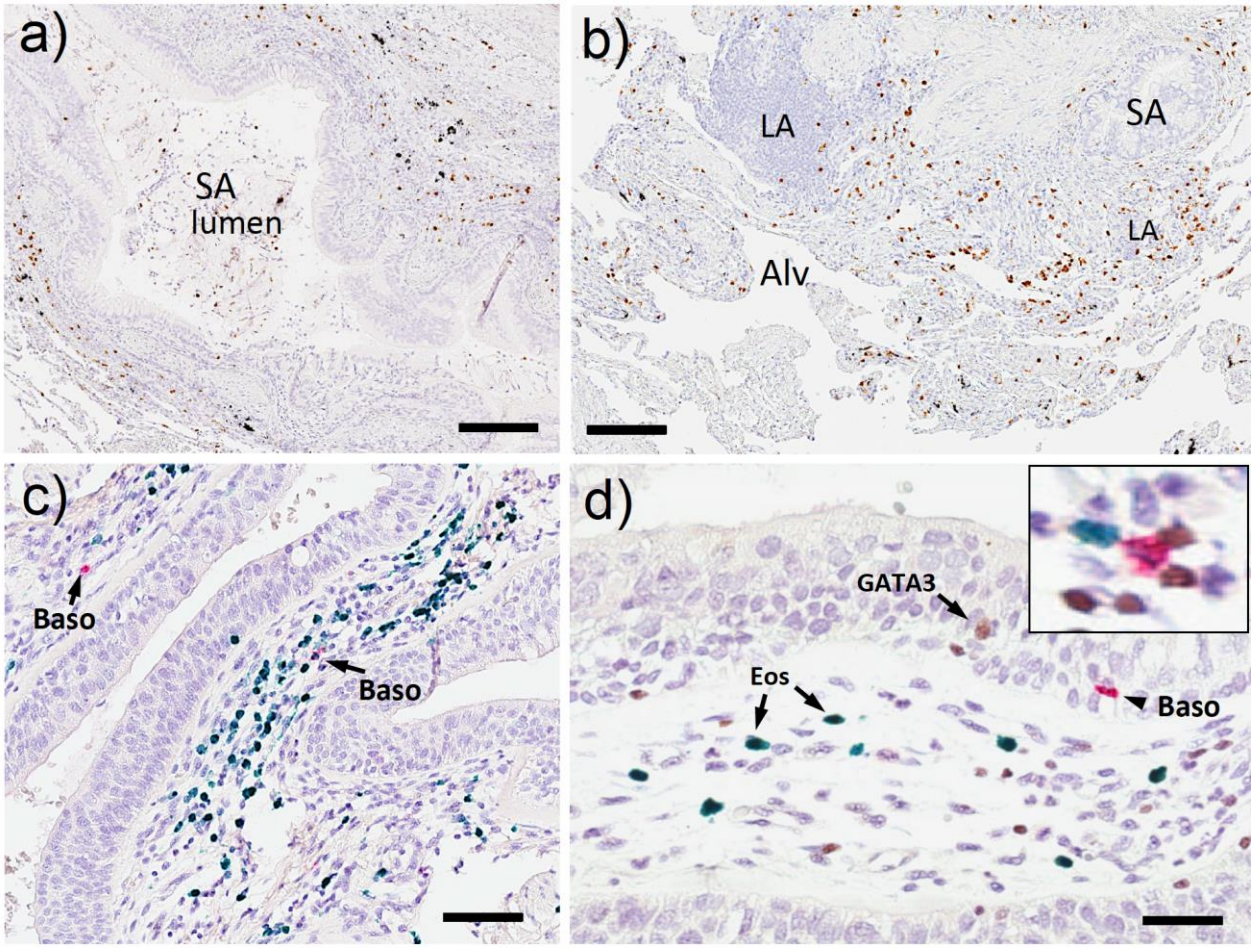
a)
SA
lumen
b)
LA
SA
LA
Alv
c)
Baso
Baso
d)
GATA3
Eos
Baso

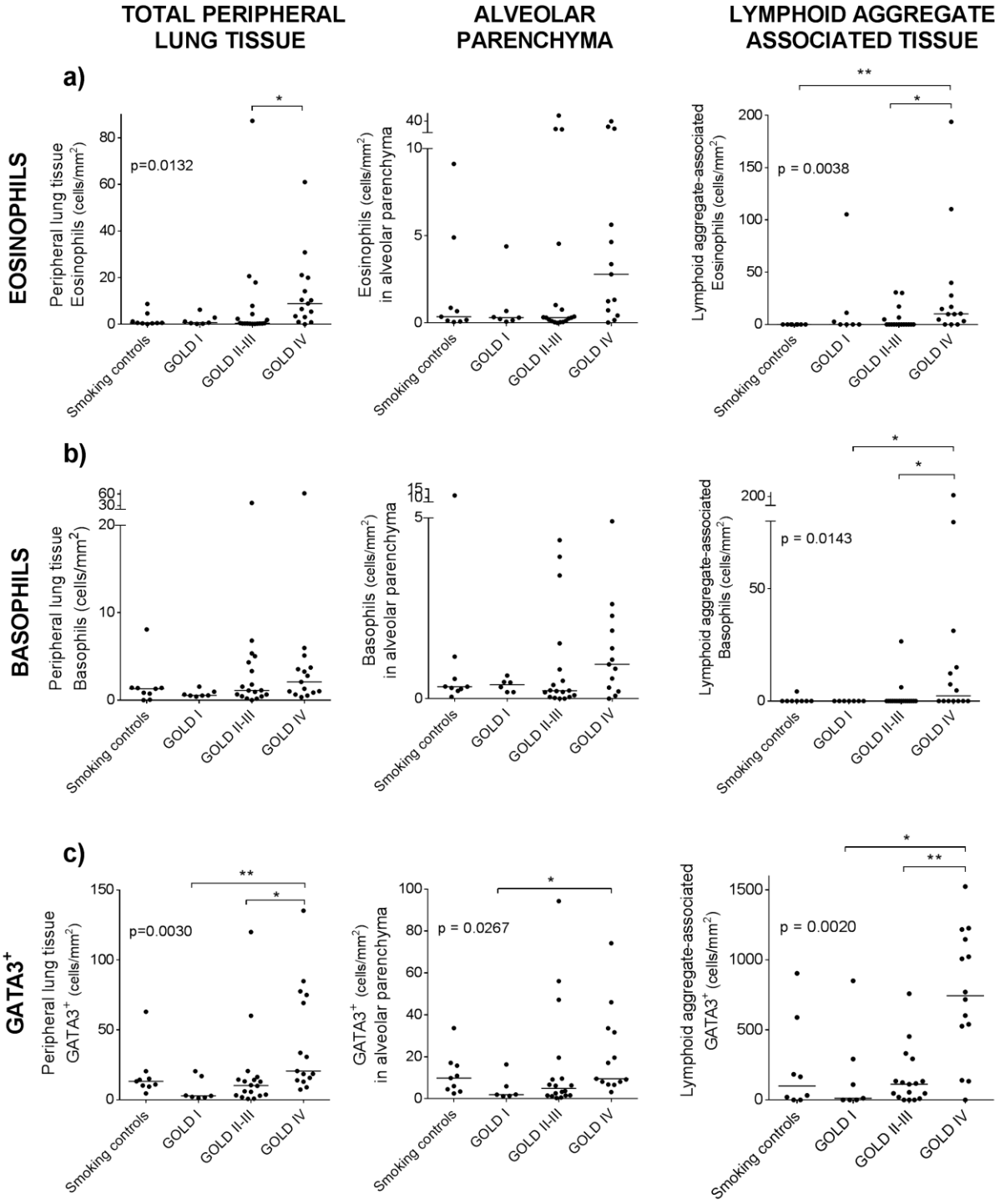
TOTAL PERIPHERAL LUNG TISSUE
ALVEOLAR PARENCHYMA
LYMPHOID AGGREGATE ASSOCIATED TISSUE
a)
EOSINOPHILS
Peripheral lung tissue Eosinophils (cells/mm2)
p=0.0132
Eosinophils (cells/mm2) in alveolar parenchyma
Lymphoid aggregate-associated Eosinophils (cells/mm2)
p = 0.0038
b)
BASOPHILS
Peripheral lung tissue Basophils (cells/mm2)
Basophils (cells/mm2) in alveolar parenchyma
Lymphoid aggregate-associated Basophils (cells/mm2)
p = 0.0143
c)
GATA3+
Peripheral lung tissue GATA3+ (cells/mm2)
p=0.0030
GATA3+ (cells/mm2) in alveolar parenchyma
p = 0.0267
Lymphoid aggregate-associated GATA3+ (cells/mm2)
p = 0.0020
Smoking controls
GOLD I
GOLD II-III
GOLD IV

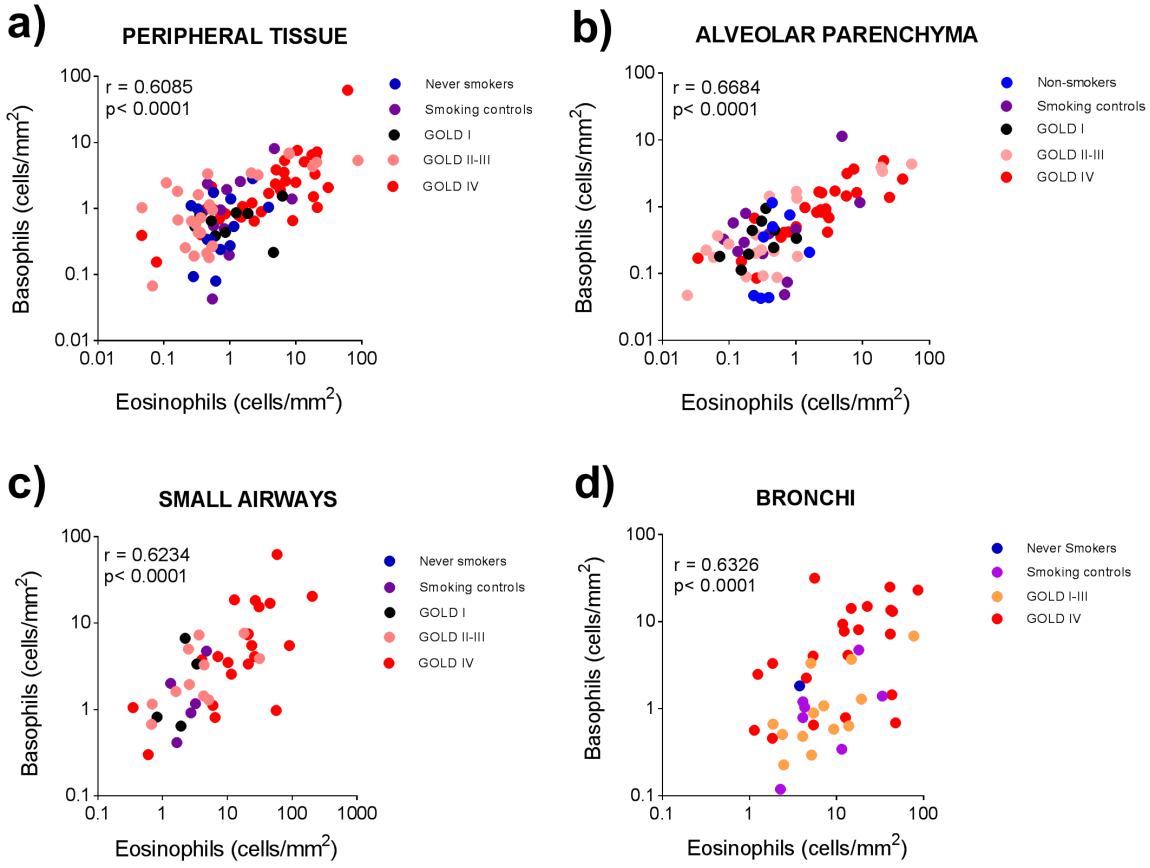
a)
PERIPHERAL TISSUE
r = 0.6085
p< 0.0001
Never smokers
Smoking controls
GOLD I
GOLD II-III
GOLD IV
Basophils (cells/mm2)
Eosinophils (cells/mm2)
b)
ALVEOLAR PARENCHYMA
r = 0.6684
p< 0.0001
Non-smokers
Smoking controls
GOLD I
GOLD II-III
GOLD IV
Basophils (cells/mm2)
Eosinophils (cells/mm2)
c)
SMALL AIRWAYS
r = 0.6234
p< 0.0001
Never smokers
Smoking controls
GOLD I
GOLD II-III
GOLD IV
Basophils (cells/mm2)
Eosinophils (cells/mm2)
d)
BRONCHI
r = 0.6326
p< 0.0001
Never Smokers
Smoking controls
GOLD I-III
GOLD IV
Basophils (cells/mm2)
Eosinophils (cells/mm2)

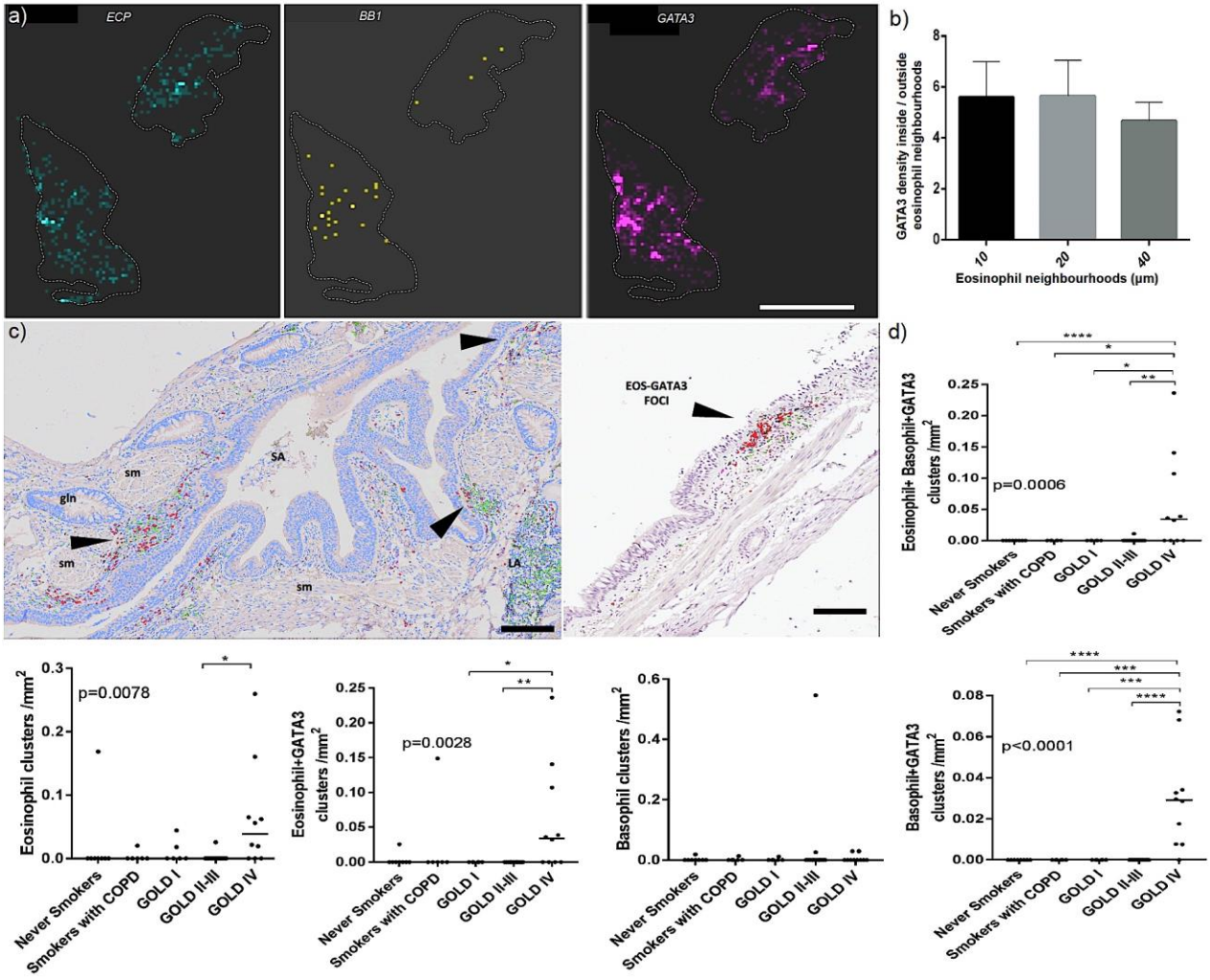
a)
ECP
BB1
GATA3
b)
GATA3 density inside / outside eosinophil neighbourhoods
Eosinophil neighbourhoods (µm)
c)
SA
sm
gln
LA
EOS-GATA3 FOCI
d)
Eosinophil+ Basophil+GATA3 clusters /mm2
p=0.0006
Eosinophil clusters /mm2
p=0.0078
Eosinophil+GATA3 clusters /mm2
p=0.0028
Basophil clusters /mm2
Basophil+GATA3 clusters /mm2
p<0.0001
Never Smokers
Smokers with COPD
GOLD I
GOLD II-III
GOLD IV

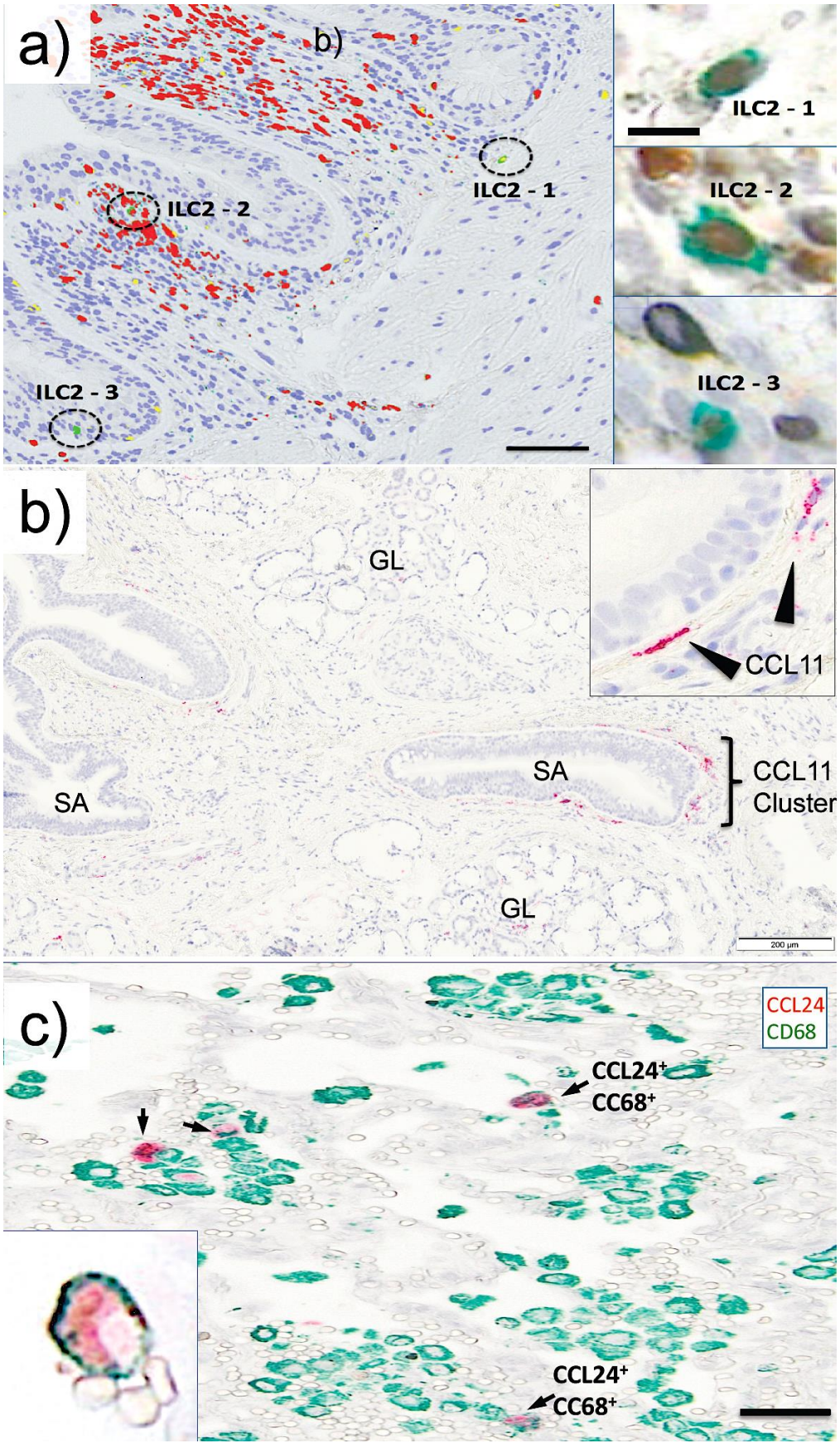
a)
b)
ILC2 - 1
ILC2 - 2
ILC2 - 3
ILC2 - 1
ILC2 - 2
ILC2 - 3
b)
GL
CCL11
SA
SA
CCL11
Cluster
GL
200 µm
c)
CCL24
CD68
CCL24+
CC68+
CCL24+
CC68+

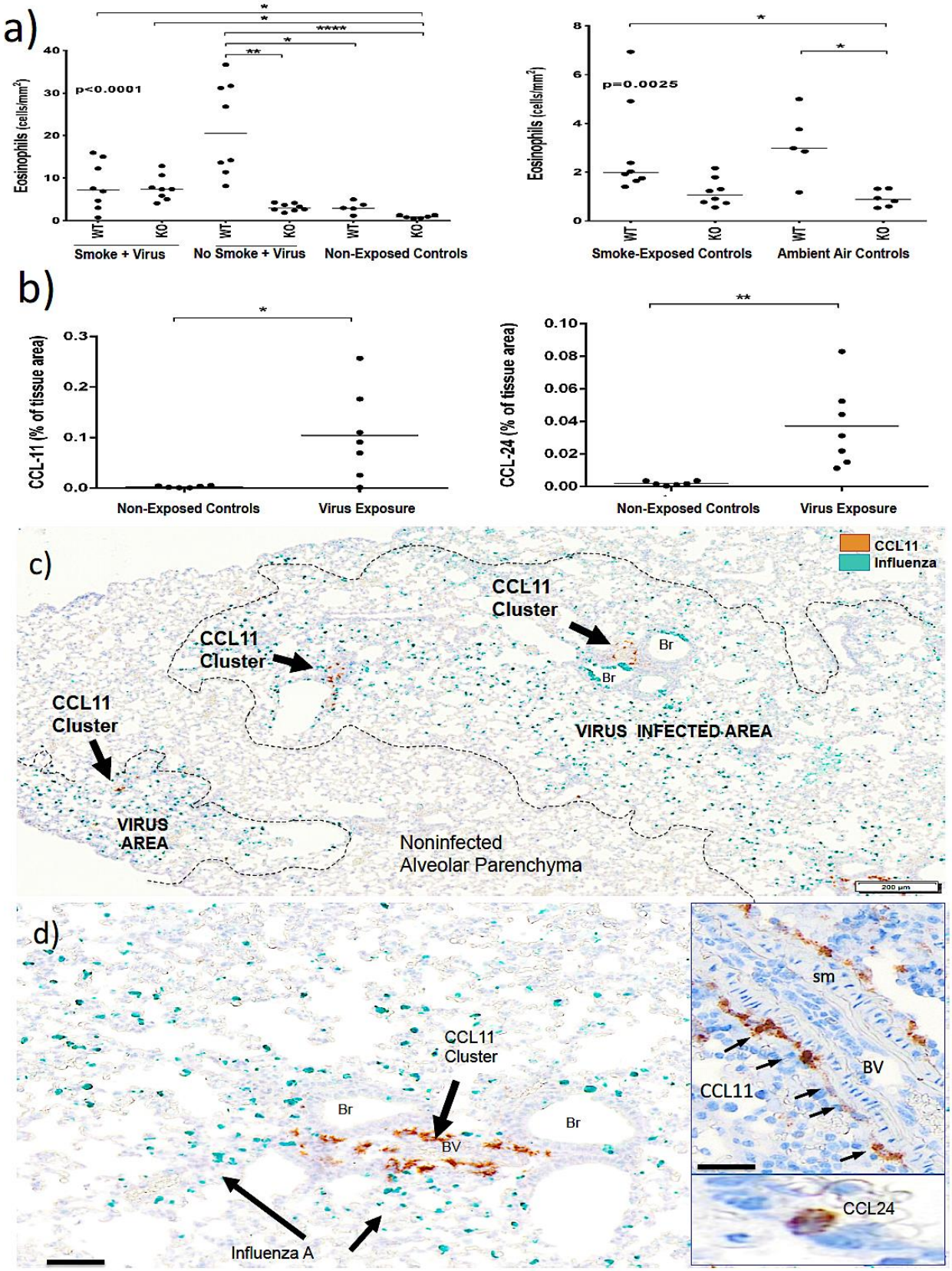
a)
Eosinophils (cells/mm²)
p<0.0001
WT
KO
Smoke + Virus
No Smoke + Virus
Non-Exposed Controls
p=0.0025
Smoke-Exposed Controls
Ambient Air Controls
b)
CCL-11 (% of tissue area)
CCL-24 (% of tissue area)
Non-Exposed Controls
Virus Exposure
c)
CCL11
Influenza
CCL11 Cluster
VIRUS INFECTED AREA
VIRUS AREA
Noninfected Alveolar Parenchyma
Br
200 µm
d)
CCL11 Cluster
Br
BV
Influenza A
sm
CCL11
CCL24

Appendix

Contents

Appendix 1. Complementary details on the methodology

Samples from participants

In total, 87 patients with chronic obstructive pulmonary disease (COPD) and controls were included in the study.

For the main study, which included patients with Global Initiative for Chronic Obstructive Lung Disease (GOLD) Stage I–III COPD and controls (N=57), surgical tissues were collected at Skåne University Hospital in Lund, Sweden, and processed for histologic analysis, as previously described [E1, E2]. The severity of COPD spanned from mild to very severe (GOLD I–IV). Lung resection samples were obtained from patients with mild to severe (GOLD I–III) COPD, as well as never-smokers and smoking controls, who were undergoing surgery for well-delineated tumours. Only patients with solid, well-defined tumours were included, and the present tissue samples were obtained as far from the tumour as possible. Explanted lung tissue from lung transplantation surgery was obtained from patients with very severe (GOLD Stage IV) COPD. For all groups, multiple lung tissue slices (approximately 15-mm thick) were immediately immersed in standard 4% buffered paraformaldehyde fixative after surgery. After fixation for approximately 24 hours, the tissues were trimmed into blocks, dehydrated, and embedded into paraffin blocks containing multiple anatomic regions of the lungs (alveolar parenchyma, bronchioles and pulmonary vessels). Separate large airway blocks (i.e., bronchi) were obtained from the explanted lungs (GOLD IV COPD patients) only. Importantly, the tissue preparation procedures were the same for all patient groups.

Inclusion criteria for the patients with COPD were a significant history of tobacco smoking and spirometrically defined COPD diagnosis according to GOLD guidelines. Thus, all included patients had a persistent airflow obstruction (forced expiratory volume in 1 second/forced vital capacity <0.7). Exclusion criteria were any atopy or allergic disease as well as any non-COPD airway-related disease (including any physician-diagnosed asthma and upper airway conditions such as rhinitis or nasal polyposis). Smoker or never-smoker control patients had no history of respiratory disease and no symptoms of infections for at least 4 weeks prior to surgery.

In additional to the surgical samples, bronchial biopsies were collected from 30 separate patients with COPD (GOLD I–II; n=13) and smoker and never-smoker controls (n=17) to increase the number of bronchial samples and available samples with appropriate messenger ribonucleic acid (mRNA)–preserved tissues for *in-situ* hybridisation (ISH). These patient groups and clinical characteristics are presented in Table E2. Bronchoscopy was performed after local anaesthesia with a flexible bronchoscope (Olympus IT160, Tokyo, Japan). Before bronchoscopy, the patients received oral midazolam (1 mg/10 kg) and intravenous (IV) Glykopyrron (0.4 mg). Local anaesthesia was given as Xylocain spray: local and through-spray catheter. Just before the procedure, alfentanyl (0.1–0.2 mg/10 kg) was given intravenously and extra intravenous midazolam was given when needed. Central airway biopsies were taken from the segmental or subsegmental carina in the lower and upper right lobe. Oxygen was given as needed during and after the procedure.

All clinical procedures were performed at the Department of Thoracic Surgery or Department Respiratory Medicine and Allergology, Lund/Skåne University Hospital, Sweden, and all

procedures were approved by the local Swedish Research Ethics Committee in Lund, Sweden. All patients signed informed consent to participate.

Immunohistochemistry

After antigen retrieval in a PT Link machine (Dako, Glostrup, Denmark), tissue sections were subjected to double and triple immunostaining using an automated immunohistochemistry robot (Autostainer Plus, Dako), as previously described [E1, E2]. For the main analysis, a triple immunohistochemistry (IHC) protocol was used to simultaneously detect eosinophils, basophils, and the Th_2 surrogate marker, GATA3 [E3, E4].

Each slide was incubated in dual endogenous enzyme-blocking reagent for 10 minutes to suppress endogenous alkaline phosphatase and peroxidase in paraffin-embedded tissue sections. The section was incubated for 1 hour in diluted antibodies against GATA3, followed by incubation for 30 minutes with polymer horseradish peroxidase (HRP)-linked secondary antibodies (EnVision™ G|2 Doublestain System Rabbit/Mouse, K5361, Dako). GATA3 cells were visualised using diaminobenzidine (DAB) (brown-coloured product, 3,3' DAB, K3468, Dako). Slides were rinsed with buffer after each step, and they were rinsed with distilled water after tissue sections were subjected to a chromogen.

Next, the sections were subjected to multiple staining with denaturing solution (DNS001H, L, Biocare Medical, Concord, CA, USA) for 5 minutes. This step was performed to denature residual antibodies to avoid cross reactivity. Tissue sections were further incubated with primary antibodies against eosinophil cationic protein (ECP) for 1 hour, followed by incubation for 30 minutes with polymer HRP-linked secondary antibodies (EnVision™ Peroxidase/DAB Detection System Kit, Rabbit/Mouse, K5007, Dako). Green-coloured

eosinophils were detected using Vina Green™ (Biocare Medical) as chromogen for this enzyme. This was followed by a 5-minute blocking and denaturing step, as previously mentioned.

For the last step, tissue sections were incubated for 1 hour in diluted BB1 antibodies followed by incubation for 1 hour with anti-mouse polymer alkaline phosphatase (EnVision G|2 Doublestain System Rabbit/Mouse, K5361, Dako). These basophils were visualised using the Liquid Permanent Red Substrate Kit (K0640, Dako). Slides were then rinsed in distilled water, counterstained with Mayer's hematoxylin solution (Sigma-Aldrich, Saint Louis, MO, USA), and mounted with Pertex® (Mitsui & Co., Ltd., Toyko, Japan).

Th_2 lymphocytes were immune-stained and identified as $GATA3^+$, $CD4^+$ cells. Type 2 innate lymphoid cells were identified as lineage-negative, $CD25^+$, $GATA3^+$ cells, as recently described [E5]. The proportion and relative abundance of Th2 vs. ILC2 cells were quantified in eosinophil-high COPD patients and expressed as percentage (%) ILC2 (and Th2 cells) of the total sum of ILC2 and Th2 cells.

Several standard IHC cell markers were also used for general immune cell exploration and to identify chemokine-expressing cells. All antibodies used have been extensively validated for use in clinical diagnosis or research and are listed in Supplemental Table E1.

In-Situ Hybridization

Human and mouse eotaxin-1 (CCL11) and eotaxin-2 (CCL24) mRNA were visualised using the RNAscope 2.5 formalin-fixed paraffin-embedded assay kit (Advanced Cell Diagnostics, Hayward, CA, USA) [E6, E7]. Sections were incubated with endogenous enzyme block,

boiled in pretreatment buffer, and treated with protease prior to target probe hybridization (CCL11, CCL24). The target RNA was then amplified using a series of amplification solutions and visualised with coloured chromogen [E6, E7].

Quantitative immunohistochemistry and computerised image analysis

Large IHC- and ISH-stained sections were digitised using a ScanScope slide scanner (Aperio Technologies, Vista, CA, USA). The high-resolution >300 MB images were subjected to computerised image analysis. Briefly, the immunoreactivity and detection chromogens were automatically detected and were quantified automatically by colour segmentation, and the total amount of marker-positive pixels were related and normalised to the tissue background pixels in the analysed region (Visiomorph™ v 4.6.3.857, Visiopharm®, Hoersholm, Denmark) [E8]. For the main study and bulk quantification of the eosinophil, basophil, and GATA3 triple-stained sections, locked threshold values and colour segmentation algorithms were set to automatically detect and quantify each chromogen without any overlap (brown DAB chromogen for GATA3, Vina Green™ for eosinophils/EG2, and permanent red substrate-chromogen for basophils/BB1).

In order to analyse distinct tissue regions, the epithelium, airway wall, pulmonary vessels, alveolar parenchyma, and lymphoid, aggregates were delineated on blinded digitalised sections by manual cursor tracing. For each participant in the main study, several large sections containing bronchioles, pulmonary vessels, and alveolar parenchyma were analysed from 2–3 separate peripheral lung regions. In total, 373 small airways (bronchioles) were analysed, derived from the control (n=93), GOLD I–III (n=167), and GOLD IV COPD (n=123) groups. For all airways, the total airway wall, the epithelial lining, and entire subepithelial tissue were analysed. The cell density in each compartment was calculated as

the number of cells/assessed tissue area. A similar approach was used for peripheral tissues. Peripheral lung tissue was defined as the more distal tissue that remains after removing any large airways or large pulmonary vessels during the gross dissections (i.e., large sections of mainly alveolar parenchyma but with occasional smaller blood vessels, small airways, lymphoid aggregates, and small fibrotic lesions). At least three separated lung regions (and three bronchial blocks) were assessed from each patient in the GOLD IV category, whereas at least two regions were assessed in the other patient groups. Alveolar parenchyma was defined as the alveolar tissue only (e.g., after small airways and larger vessels have been excluded from the analysis by manual cursor tracing), whereas lymphoid tissue–associated cells referred to cells in the tissue directly surrounding ectopic lymphoid tissue. Importantly, for all compartments, the analysis of cell density was expressed as cells/area of proper tissue (after any air spaces, vessel lumen, or larger tissue cracks have been segmented and excluded by a tissue detection algorithm, including removal of the white "air" background).

Eosinophil and basophil clustering

Semi-manual quantification of clusters

Initial manual inspection of the eosinophil, basophil, and GATA3-stained sections revealed several cases of marked patchiness and cell clustering (exemplified in Figure E3). To get a quantitative estimate of such eosinophil and/or basophil clusters, they were counted manually on blinded high-resolution digital image files of the EG2, BB1, and GATA3 triple-stained sections. For this analysis, a cluster was defined as presence of multiple immuno-stained cells (eosinophils or basophils) within a defined circle (100 μm in diameter) with a clear absence of cells in the neighbourhood outside the circle. Such eosinophil and/or basophil clusters were also evaluated for their content of any GATA3-positive cells and expressed as average of clusters/cm lung tissue.

Point pattern analysis to confirm spatial eosinophil clustering

The manual quantification of cell eosinophil clusters was also complemented with spatial statistics and point pattern analysis. Briefly, X,Y coordinates were generated from computer-segmented, immune-stained eosinophils (CC, Medetect, Lund, Sweden) and were used for point pattern analysis of degree of clustering. The statistical models selected for this (nearest neighbour distance analysis and Ripley's K point pattern analysis) require a predominantly convex domain of background tissue and sufficient eosinophils within the selected region of interest, limiting the analysis to six cases from the GOLD IV COPD group. After a Donnelly's correction for edge effect [E9], nearest neighbour distance analysis revealed a highly spatially clustered pattern ($p<0.001$) in the analysed cases.

Spatial analysis of co-clustering of eosinophil and GATA3$^+$ cells

A neighbourhood analysis principle was used to analyse the density of GATA3$^+$ cells inside and outside eosinophil microenvironments in numerous double-stained, eosinophil-rich sections. Each EG2-immunoreactive eosinophil was identified by computerised image analysis, as previously described. Next, a virtual circle with a fixed radius was created around each eosinophil (Cell Community Viewer, CCV 1.22, Medetect, Lund, Sweden) (Figure E1). Three radii were applied (10 μm, 20 μm, and 40 μm), corresponding to three defined sizes of eosinophil neighbourhoods. Using information about GATA3-segmented marker objects, quantitative data of GATA3 density inside and outside eosinophil neighbourhoods were automatically generated and used to calculate the density of GATA3 within and without eosinophil microenvironments, expressed as the ratio: $GATA3^{\text{Eos neighbourhood}}$ / $GATA3^{\text{Non-eos neighbourhood}}$. For each analysed image, the mean density was calculated as total GATA3 immunoreactivity area/total eosinophil neighbourhood area (or total noneosinophil area in the case of $GATA3^{\text{Non-eos}}$).The hypothesis that the eosinophil tends to occur in spatial regions

with a particularly high density of GATA3+ cells was also tested using Monte Carlo simulations, as previously described for eosinophil and ILC2 co-distribution [E5]. Briefly, using the MOSAIC Interaction Analysis Plugin for Fuji/ImajeJ [E10), a circular neighbourhood was defined around each of the eosinophil locations (x,y coordinate). The number of GATA3 in each of these neighbourhoods was counted and added to produce a count for the entire group of cells. The distribution of the simulation round GATA3 counts under the null hypothesis of random placement was determined by 10^4 simulation rounds of eosinophil locations randomly placed within the study area and calculating the group GATA3 count measure for each simulated group. A simple proportional edge correction was applied to neighbourhood counts when part of the circular neighbourhood fell outside the study area.

Analysing the sections with patchy eosinophilia, the null hypothesis could be rejected with a significance level of $p<0.001$, showing that the density of GATA3 cells around the eosinophil locations is indeed significantly higher than would be expected by chance.

Appendix 2. Results: supplemental images

In total, 75 patients with chronic obstructive pulmonary disease (COPD) and controls were included in the study. For the main study, which included patients with COPD and controls (N=45), surgical tissues were collected at Skåne University Hospital in Lund, Sweden, and processed for histologic analysis, as previously described [E1, E2]. Patient groups and clinical characteristics of those in the main study are presented in Table E2.

Bronchial biopsies and tissues samples from 30 separate patients (n=13) and controls (n=17) were used to collect appropriate messenger ribonucleic acid (mRNA)-preserved tissues for *in-situ* hybridisation (ISH). These patient groups and clinical characteristics are presented in Table E2.

The following supplemental images are presented to support the Results section in the main manuscript:

- Micrographs illustrating the principle of automatic detection of eosinophil neighbourhoods in order to reveal a spatial link between $GATA3^{+}$ cells and eosinophil microenvironments (Figure E1)
- Density of eosinophils and basophils in the bronchial biopsy cohort (Figure E2)
- Greater magnification of a spatially distinct eosinophil and GATA3-rich microenvironment (Figure E3)
- Co-emergence of CCL-24 (eotaxin 2) and eosinophil in influenza A–challenged mouse lungs (Figure E4)

Table E1. Antibodies for Immunohistochemical Analysis

Antigen	Clone	Host/ Isotype	Supplier	Antigen Retrieval	Dilution	Against	Secondary Antibody, EnVision™ Detection System Kit, Dako
ECP	EG2	Mouse/ $mIgG_1$	Diagnostics Development	Low pH[#] PT	1:500	Eosinophils	Polymer anti-mouse HRP, K8010
BB1	BB1	Mouse/ $mIgG_2a$	Provided by Dr. Andrew Walls, Southampton, UK	Low pH[#] PT	1:50	Basophils	Polymer anti-mouse AP, K5361
GATA3	L50-823	Mouse/ $mIgG_1\kappa$	BD Biosciences BD Pharmingen™	Low pH[#] PT	1:2,000	Transcription factors	Polymer anti-mouse HRP, K5361
CD68	PG-M1	Mouse/ $mIgG_3\kappa$	Dako	Low pH PT	1:200	Monocytes and macrophages	Polymer anti-mouse , HRP K5361
CD31	C8/ 1448	Mouse/ Ig	Dako	Low pH PT	1 :100	Endothelial cells	Polymer anti-mouse HRP, K5361
CD8	JC70A	Mouse	Dako	Low pH PT	1 :640	Cytotoxic T cells	Polymer anti-mouse HRP, K5361
CD 25	4C9	Mouse/ $mIgG_2b$	Novocastra NCL/Leica	Low pH PT	1:50	IL-2 receptors	Polymer anti-mouse HRP, K5361
GATA3	L50-823	Mouse/ $mIgG_1\kappa$	BD Biosciences	Low pH PT	1:1,000	Transcription factors	Polymer anti-mouse HRP, K5361
CD4	4B12	Mouse/ $mIgG_1$	Novocastra NCL/Leica	High pH[¶]	1:50	T-helper cells	Polymer anti-mouse HRP, K5361
GATA3	L50-823	Mouse/ $mIgG_1$	BD Biosciences	High pH[¶]	1:2,000	Transcription factors	Polymer anti-mouse HRP, K5361

[#]EnVision™ FLEX Target Retrieval Solution, Low pH 6.1, K8005, Dako.
[¶]EnVision™ FLEX Target Retrieval Solution, High pH 9, K8010, Dako.

Table E2. Study Participant Demographics (Bronchoscopy Study)

Parameters	**Former Smokers**	**COPD (GOLD I–III[#])**	**Never-smokers**
Patients	9	13	8
Age, years	67 (64–71)	66 (45–74)	23 (21–39)
Sex, male/female	6/3	9/4	3/5
Body mass index, kg/m^2	27.14 (13.50–33.20)	26.03 (18.65–30.37)	23.01 (19.38–27.10)
Smoking history, pack-years	30 (17–48)	36 (14–159)	NA
$FEV_{1,}$ L (after β_2-agonist)	3.2 (1.9–3.7)	1.6 (0.7–2.6)	3.6 (2.3–5.3)
FEV_1, % predicted (after β_2-agonist)	91.9 (88.1–132.3)	52.0 (28.3–82.1)	98.05 (72.10–116.40)

COPD, chronic obstructive pulmonary disease; FEV_1, forced expiratory volume in 1 second; GOLD, Global Initiative for Chronic Obstructive Lung Disease; NA, not applicable. Values are median (range) or n.

[#]The COPD GOLD I–III cohort composition is: GOLD I (n=1), GOLD II (n=8), and GOLD III (n=4).

Appendix 3. Figures

Figure E1. Micrographs illustrating the principle of automatic detection of eosinophil neighbourhoods in order to reveal a spatial link between GATA3^{+} cells and eosinophil microenvironments. (a and b) Vina green chromogen-stained eosinophils have been detected with colour segmentation and automatically labelled with a dark blue pseudo colour. The turquoise areas represent the automatically generated virtual circular "eosinophil neighbourhood" areas that are created around each eosinophil object. (c and d) Low-power overview images of bronchioles in COPD lungs where 40-µm virtual circular eosinophil neighbourhoods are labelled yellow. Computer-segmented eosinophils are labelled blue and DAB-positive GATA3 cells green. The mucosal subepithelial lamina propria tissue is labelled dark grey.

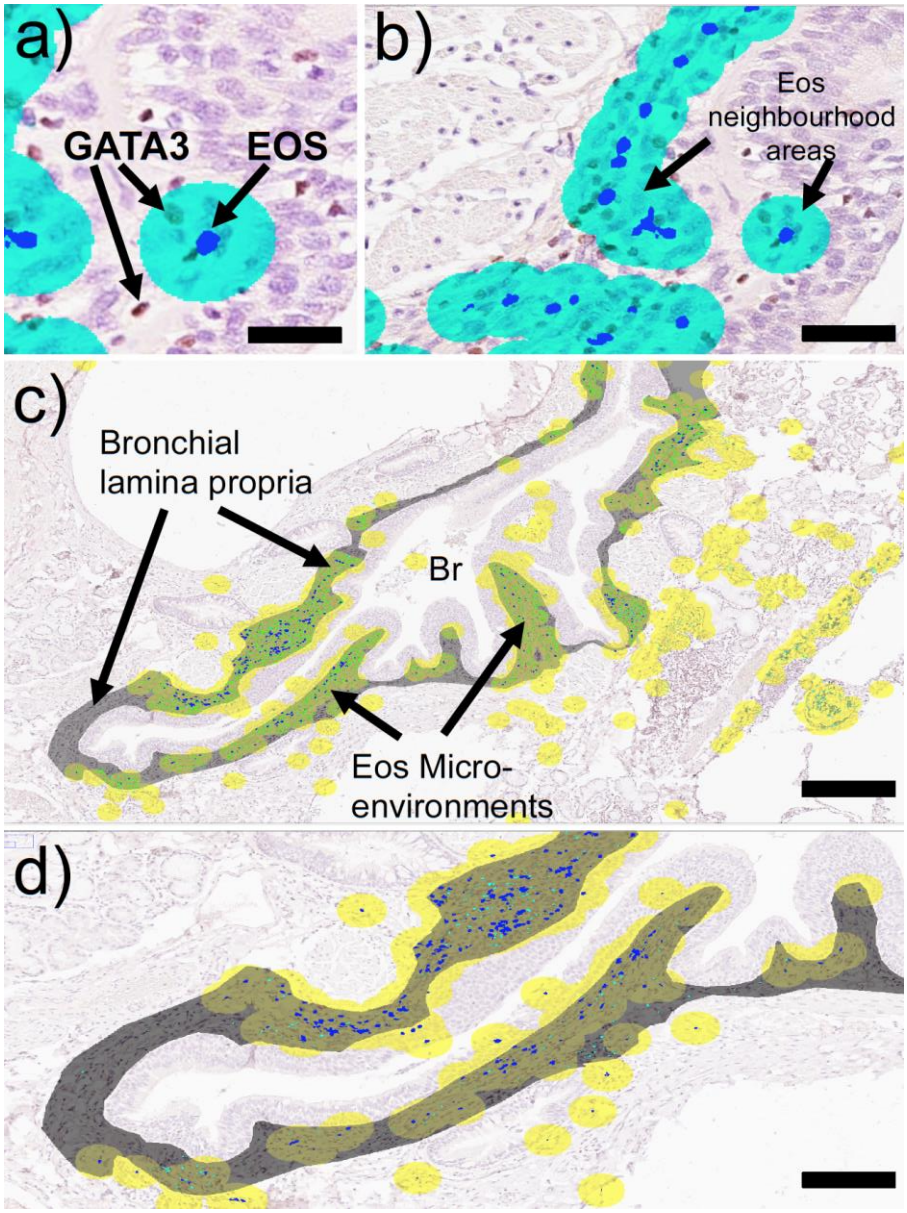

Scale bars: a=25 µm, b=40 µm, c=80 µm, d=65 µm.
COPD, chronic obstructive pulmonary disease; DAB, diaminobenzidine.

Figure E2. Panels a and b show eosinophil and basophil numbers in the separate bronchial biopsies, collected from the bronchoscopy study (from GOLD I–III patients with COPD). Dots represent mean patient values and horizontal dashes represent group mean values. Panels in C show the tissue density of eosinophils, basophils, and GATA3 in bronchioles (small airways) and bronchi in very severe COPD.

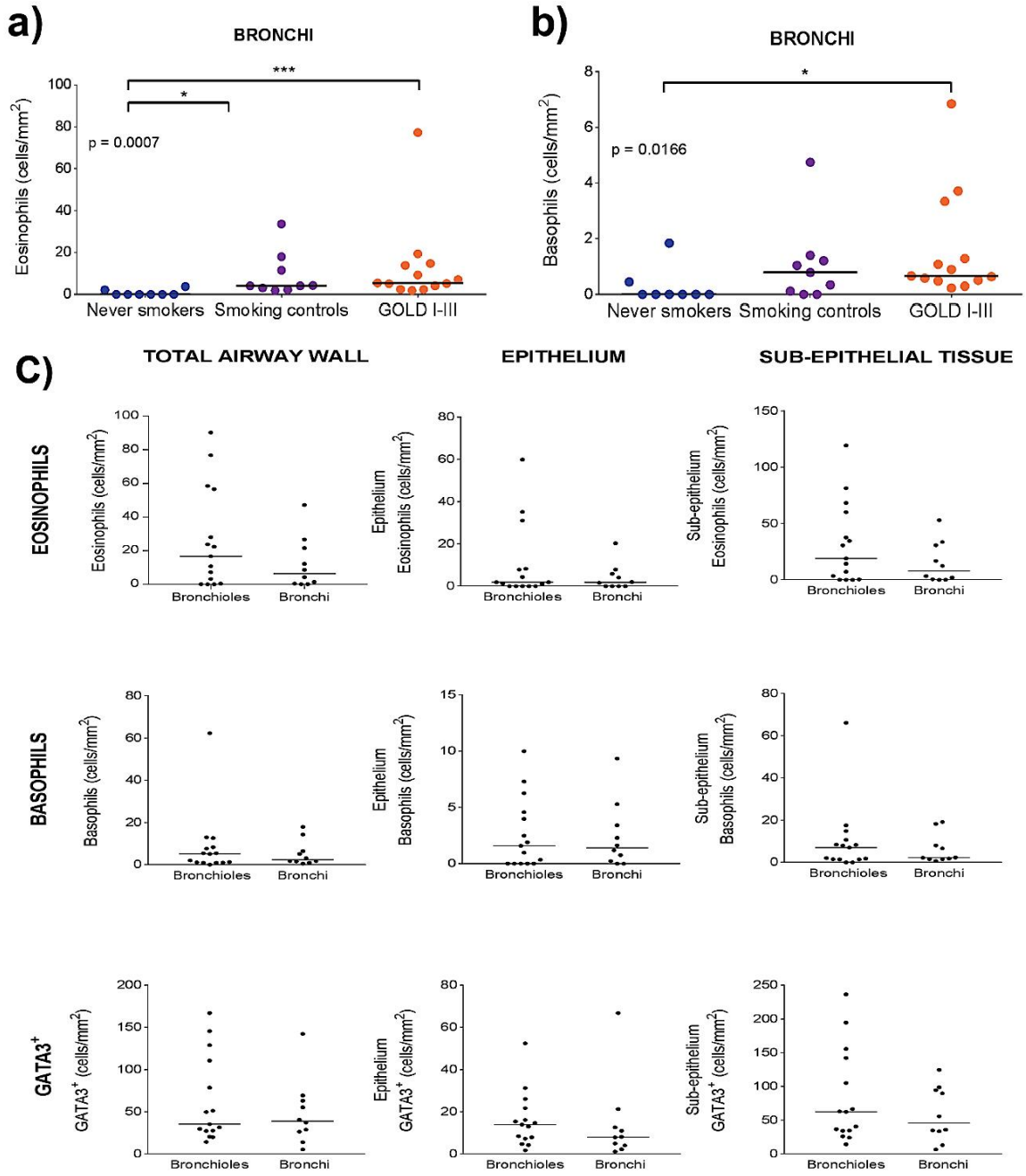

Asterisks denote degrees of statistical significance between groups: *p<0.05; ***p<0.001. P-values quoted in the figure represent overall statistical difference between patients with COPD and controls, as determined by a non-parametric Kruskal-Wallis one-way ANOVA with Dunn's multiple comparison *post-hoc* test (mean rank of each subgroup is compared with every other subgroup). No statistical differences were found between bronchi and bronchioles in C.

COPD, chronic obstructive pulmonary disease; GOLD, Global Initiative for Chronic Obstructive Lung Disease.

Figure E3. (a) Multi-stained tissue section of a small COPD bronchi that exemplifies a spatially distinct eosinophil and GATA3-rich foci, labelled here as a Th_2-skewed pocket. Eosinophils were identified by EG2 immunoreactivity and pseudo coloured red whereas $GATA3^+$ cells are marked bright green. (b) Greater magnification of the same section and Th_2 pocket, where cell nuclei also have been pseudo coloured (blue).

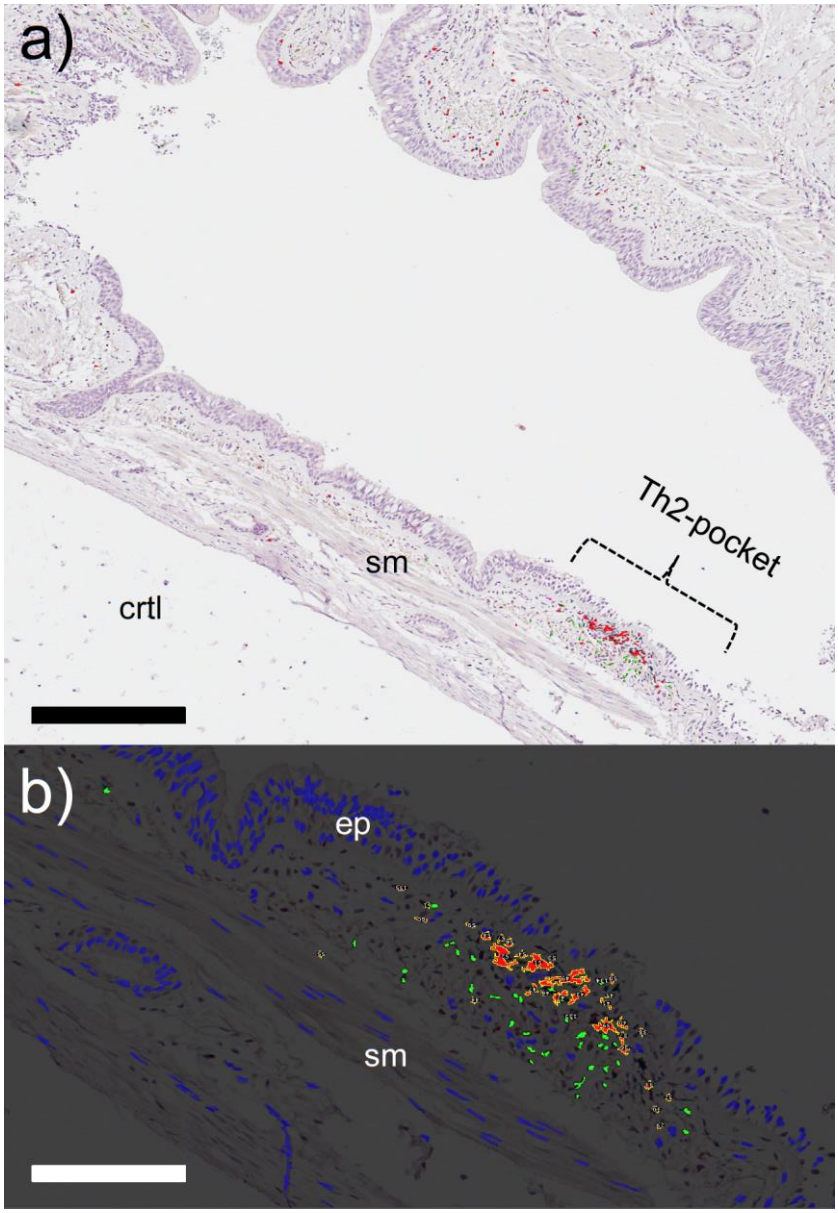

Scale bars: a=350 μm, b=150 μm.
COPD, chronic obstructive pulmonary disease; ctrl, bronchial cartilage; ep, bronchial epithelium; sm, smooth muscle.

Figure E4. Spatial correlation between localized CCL11 (eotaxin 1) and CCL-24 (eotaxin 2) and eosinophils in localized influenza A–infected mouse lung areas. Examples of percentages of tissue area positive for ISH-detected CCL11 (a) and CCL24 (b) mRNA in virus-low (grey) and virus-high (black) lung regions in representative individual mice. (c) Bright field image of CCL-24 mRNA, as detected by *in-situ* hybridisation and brown DAB detection chromogen. (d) The same lung area stained for eosinophils (green fluorescence; DAPI was used for blue cell nuclei detection).

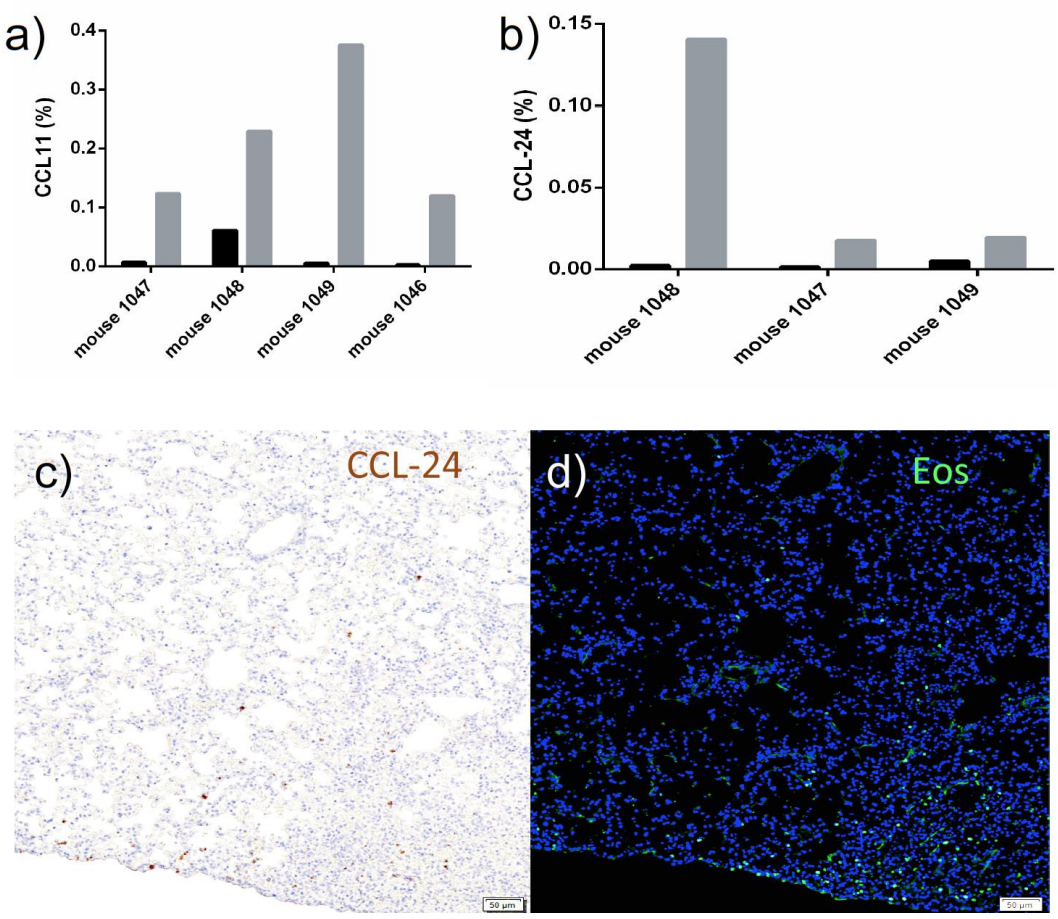

Scale bars: 50 µm.
DAB, diaminobenzidine; DAPI, 4',6-diamidino-2-phenylindole; ISH, in situ hybridisation; mRNA, messenger ribonucleic acid.

Appendix 4. References

E1. Roos AB, Sanden C, Mori M, et al. IL-17A is elevated in end-stage chronic obstructive pulmonary disease and contributes to cigarette smoke-induced lymphoid neogenesis. *Am J Respir Crit Care Med* 2015; 191: 1232–1241.

E2. Mori M, Andersson CK, Svedberg KA, et al. Appearance of remodelled and dendritic cell-rich alveolar-lymphoid interfaces provides a structural basis for increased alveolar antigen uptake in chronic obstructive pulmonary disease. *Thorax* 2013; 68: 521–531.

E3. Das J, Chen CH, Yang L, et al. A critical role for NF-kappa B in GATA3 expression and TH2 differentiation in allergic airway inflammation. *Nat Immunol* 2001; 2: 45–50.

E4. Nakayama T, Hirahara K, Onodera A, et al. Th2 Cells in Health and Disease. *Annu Rev Immunol* 2016; 35: 53–84.

E5. Bal SM, Bernink JH, Nagasawa M, et al. IL-1beta, IL-4 and IL-12 control the fate of group 2 innate lymphoid cells in human airway inflammation in the lungs. *Nat Immunol* 2016; 17: 636–645.

E6. Wang F, Flanagan J, Su N, et al. RNAscope: a novel in situ RNA analysis platform for formalin-fixed, paraffin-embedded tissues. *J Mol Diagn* 2012;14:22–29.

E7. Silver JS, Kearley J, Copenhaver AM, et al. Inflammatory triggers associated with exacerbations of COPD orchestrate plasticity of group 2 innate lymphoid cells in the lungs. *Nat Immunol* 2016;17: 626–635.

E8. Bergqvist A, Andersson CK, et al. Alveolar T-helper type-2 immunity in atopic asthma is associated with poor clinical control. *Clin Sci (Lond)* 2015;128:47–56.

E9. Hammer Ø. New methods for the statistical analysis of point pattern alignments. *Comput Geosci* 2009; 35: 659–666

E10. Shivanandan A, Radenovic A, Sbalzarini IF. MosaicIA: an ImageJ/Fiji plugin for spatial pattern and interaction analysis. *BMC Bioinformatics* 2013;14:349.